

This work was written as part of one of the author's official duties as an Employee of the United States Government and is therefore a work of the United States Government. In accordance with 17 U.S.C. 105, no copyright protection is available for such works under U.S. Law.

Public Domain Mark 1.0

<https://creativecommons.org/publicdomain/mark/1.0/>

Access to this work was provided by the University of Maryland, Baltimore County (UMBC) ScholarWorks@UMBC digital repository on the Maryland Shared Open Access (MD-SOAR) platform.

Please provide feedback

Please support the ScholarWorks@UMBC repository by emailing scholarworks-group@umbc.edu and telling us what having access to this work means to you and why it's important to you. Thank you.



Long-term variation of aerosol optical properties associated with aerosol types over East Asia using AERONET and satellite (VIIRS, OMI) data (2012–2019)

Sujin Eom^a, Jhoon Kim^b, Seoyoung Lee^b, Brent N. Holben^c, Thomas F. Eck^c, Sung-Bin Park^a, Sang Seo Park^{a,*}

^a Department of Urban and Environmental Engineering, Ulsan National Institute of Science and Technology (UNIST), Ulsan, Republic of Korea

^b Department of Atmospheric Sciences, Yonsei University, Seoul, Republic of Korea

^c NASA Goddard Space Flight Center, Greenbelt, MD, USA

ARTICLE INFO

Keywords:

AERONET

AOD

Aerosol type classification

OMI

VIIRS

ABSTRACT

We analyzed annual and seasonal frequency in aerosol type over an 8-year period (2012–2019) to identify aerosol parameter trends over four ground sites and country regions in Korea, China, and Japan by using the Aerosol Robotic Network (AERONET), and the satellite-based Visible Infrared Imaging Radiometer Suite (VIIRS) and Ozone Monitoring Instrument (OMI). Decreasing trends are shown for aerosol optical depth (AOD), Ångström exponent (AE), and fine mode fraction (FMF) in all countries. The decreasing trend in these data is considered to be due to a decrease in anthropogenic emissions. For the aerosol type frequency, decreases in the proportions of carbonaceous aerosols (CA) and non-absorbing aerosols (NA) were shown in the ground and satellite data, respectively. At most sites, the fractions of low AOD case (LOW) increased, whereas those of the Black and Brown Carbon (BC + BrC) category decreased. In Seoul, the fraction of LOW increased from 48.9% to 70.0%, and that of BC + BrC decreased continuously from 20.4% to 11.1% during 2012–2019. Beijing, on the other hand, showed decreasing LOW from 83.3% (2012) to 52.0% (2019), and that of BC + BrC increased significantly, from 2.4% to 26.2%. The satellite data showed that the percentage of LOW increased continuously, while that of NA aerosols decreased continuously in East Asia. A noticeable decrease in the fraction of CA was detected in China [21.5% (2013) to 11.2% (2019)]. In all countries, CA and NA aerosols had the greatest effect in winter and summer, respectively. We also detected significant differences between the fractions of NA and BC between the ground and satellite data. Changes in aerosol type and properties were observed concurrently in all ground and satellite data, and changes in aerosol type may explain the increasing and decreasing trends that we recorded for most parameters. Consistent results from both ground and satellite data suggest a steady decreasing in fine aerosol pollution in East Asia.

1. Introduction

Aerosols comprise various forms of particulate matter suspended in the air; they have important influences on the global climate and public health. Because aerosol emissions are directly related to air quality, exposure to large amounts of aerosols has adverse health effects (Kwon et al., 2002; Malilay, 1999). Segersson et al. (2017) discovered that high exposure to black carbon (BC) has increased premature mortality by up to approximately 60% in certain regions. Another study suggested that the reason why decrease in available water volume can be due to air

pollution (Givati and Rosenfeld, 2007). Additionally, the amount of visible light can be reduced under a high aerosol concentration (Tie and Cao, 2009). Reductions in visible light can have adverse effects on humans and environments; thus, there is a need to quantify the amount of aerosol in the atmosphere.

Various aerosol types are emitted from anthropogenic and natural sources (Park et al., 2003; Streets et al., 2009). For example, sea salt and dust are naturally emitted, whereas non-absorbing (NA) aerosols (e.g., sulfates and nitrates) and BC are mainly derived from anthropogenic sources (Streets et al., 2009). The presence of various aerosol types can

* Corresponding author.

E-mail address: sangseopark@unist.ac.kr (S.S. Park).

<https://doi.org/10.1016/j.atmosres.2022.106457>

Received 23 June 2022; Received in revised form 20 September 2022; Accepted 22 September 2022

Available online 27 September 2022

0169-8095/© 2022 The Author(s). Published by Elsevier B.V. This is an open access article under the CC BY license (<http://creativecommons.org/licenses/by/4.0/>).

affect the optical properties of the atmospheric layer (Li et al., 2022). Aerosols have direct and indirect effects on the radiative balance (Koch et al., 2009; Rap et al., 2013), which affects global warming and can vary according to the aerosol type (Xia, 2014). Nagorski et al. (2018) reported that the radiative forcing of BC and dust differed by approximately 10^3 fold for the same amount of aerosol. The hygroscopic growth of aerosols can affect visibility, and it varies depend on aerosol composition (Tie and Cao, 2009). Sulfate grows continuously with increasing relative humidity (RH), but BC does not grow until under 70% RH; in contrast, dust particle do not grow under any RH case (Tie and Cao, 2009). Consequently, different types of aerosols have variable impacts on the environment, and quantifying both the amount and type of aerosols are important for management of atmospheric pollution.

Based on the characteristics of aerosol optical properties, many previous studies have developed aerosol type classification algorithms (e.g., Chen et al., 2016a, 2016b; Hamill et al., 2016; Lee et al., 2010; Omar et al., 2005; Penning de Vries et al., 2015). Several studies have used in situ aerosol properties to differentiate aerosol types (e.g., Cappa et al., 2016; Cazorla et al., 2013; Kaskaoutis et al., 2021). Cazorla et al. (2013) published a classification method using columnar measurements, which was based on the absorbing Ångström exponent (AAE) and scattering Ångström exponent (SAE). Cappa et al. (2016) modified the previous algorithm using in situ measurements. This AAE-SAE algorithm was used in several studies, most of which focused on the overall characteristics of several areas (e.g. Hopner et al., 2018; Kaskaoutis et al., 2021). Several studies have examined the global and regional frequency distributions of various aerosol types according to their optical properties (e.g., Lin et al., 2022; Logothetis et al., 2020; Mok et al., 2017; Schmeisser et al., 2017), but these studies have limitations in terms of long-term variation.

Aerosol types and optical properties exhibit high spatiotemporal variability because their compositions vary according to origin (Kaskaoutis et al., 2009). Continuous changes in industrial activity can affect the long-term characteristics of aerosol emissions, as observed in several countries (Lei et al., 2011; Zhao et al., 2017). Because aerosol emission characteristics change over long periods, there is a need to obtain long-term data regarding aerosol types. Therefore, many previous studies have analyzed aerosol optical properties using long-term data or case studies of specific regions (e.g., Kim et al., 2007; Lee et al., 2007; Shin et al., 2019; Tian et al., 2020). However, fewer studies have examined long-term variations in aerosol type (e.g., Chen et al., 2020; Ou et al., 2017). Several studies have focused on aerosol emissions (e.g., Ou et al., 2017; Song et al., 2008) and aerosol characteristics in East Asia (e.g., Li et al., 2015), because aerosol types considerably vary in this region due to the diverse range of emission sources (Kang et al., 2017). Some previous studies evaluated aerosol properties over East Asia using ground and satellite data (e.g., Kim et al., 2014; Lee and Kim, 2010). During the Aerosol Characterization Experiment-Asia (ACE-Asia) conducted in 2001, aerosol characterization was conducted in East Asia. Quinn et al. (2004) noted that within this region, aerosols consist of a complex mixture of marine, pollution, volcanic and dust sources. Furthermore, in situ data for the previous period (from 2001 to 2010) showed that the ground-based mass concentration continued to decrease in East Asia (Kim et al., 2014). The increasing emission of anthropogenic fine aerosols suggested that this result was caused by the decreasing occurrence of yellow dust event (Kim et al., 2014). In addition, generally strong correlation was observed between the increase in aerosol optical depth (AOD) and the increase in sulfate (Kim et al., 2014). Until recently, it was difficult to determine whether these long-term results have had a steady effect on aerosol properties. Therefore, past studies have provided extensive aerosol data, but there have been few studies of long-term variation in aerosol types according to their optical properties (e.g., Chen et al., 2020; Ou et al., 2017).

The objective of this study was to understand the trends (over an 8-year period) of aerosol types and parameters in East Asia. Ground and satellite observation data were used in combination to identify changes

in aerosol type along with increases and decreases in aerosol optical properties. In this study, a combination of aerosol type classification algorithms was developed using Aerosol Robotic NETwork (AERONET) data, based on the results of previous studies (Cappa et al., 2016; Lee et al., 2010). For ground data analysis, the method established by Lee et al. (2010) was used to isolate mixed categories of algorithm from Cappa et al. (2016). For satellite data analysis, delicate filtering was performed using level 2 data of visible infrared imaging radiometer suite (VIIRS) and ozone monitoring instrument (OMI). This approach differed from the moderate resolution imaging spectroradiometer (MODIS)-OMI combined algorithm (MOA), which used level 3 ($1^\circ \times 1^\circ$) data of MODIS and OMI (Mok et al., 2017). Section 2 describes how these aerosol classification methods were used for ground and satellite data, respectively. Based on the results of combined analyses involving ground and satellite data, this work will suggest the direction of future studies. For example, long-term changes in aerosol type could visualize the outcomes of recent air quality-related regulations; it may be possible to establish more detailed regulations for each country in the region. Section 3 presents the study results in terms of aerosol parameter trends, as well as annual and seasonal analyses of aerosol types.

2. Data and methods

2.1. Study area

We selected four AERONET sites within three countries in East Asia for which multi-year datasets (2012–2019) were available (Fig. 1). Two of the sites, Seoul_SNU and Yonsei_University were in Seoul, Korea, with differences in latitude and longitude of $<0.2^\circ$; therefore, these sites were combined into a single ‘Seoul’ dataset. The other sites were Beijing, China, and Osaka, Japan. For the Beijing site, data from the Beijing-CAMS (39.933°N , 116.317°E) site were used for the supplement of missing data of Beijing site. Therefore, the ground sites in this study were Seoul, Beijing, and Osaka. We used polar-orbiting satellite data from the VIIRS and OMI sensors over $4^\circ \times 5^\circ$ (latitude \times longitude) areas including AERONET sites in each of the three target countries; Korea, China, and Japan (Fig. 1).

2.2. Data

Several previous studies analyzed aerosol properties in terms of optical thickness, fine particle content, absorption, and scattering (e.g., Kim et al., 2007; Lee et al., 2010). These characteristics allow the

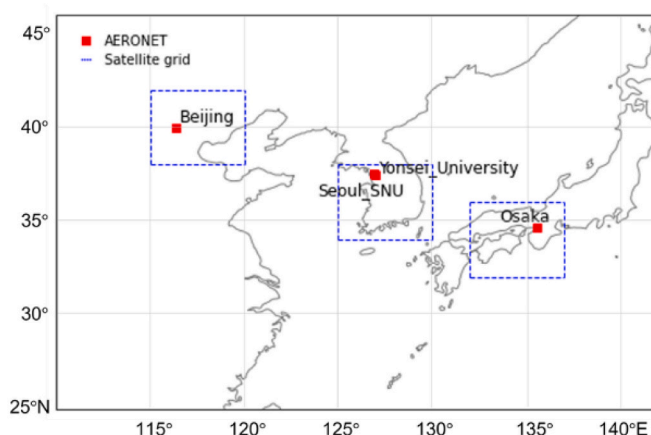


Fig. 1. Locations of AERONET observation sites [Seoul_SNU (37.458°N , 126.951°E), Yonsei_University (37.564°N , 126.935°E), Beijing (39.977°N , 116.381°E), Osaka (34.651°N , 135.591°E)] and the field of grid for satellite observations in Korea ($34^\circ\text{--}38^\circ\text{N}$, $125^\circ\text{--}130^\circ\text{E}$), China ($38^\circ\text{--}42^\circ\text{N}$, $115^\circ\text{--}120^\circ\text{E}$), Japan ($32^\circ\text{--}36^\circ\text{N}$, $132^\circ\text{--}137^\circ\text{E}$).

identification of aerosol types using classification algorithms (e.g., Ou et al., 2017; Schmeisser et al., 2017). In this study, we obtained aerosol information using both ground data and satellite data. Ground data provide accurate observations at a specific point, whereas satellite data cover a wide spatial range. Therefore, the simultaneous use of both ground and satellite observation data provides more comprehensive information about a study area; synergistic use is expected. In this study, we obtained ground data collected by AERONET (Holben et al., 1998) and satellite data collected by VIIRS and OMI during 2012–2019.

2.2.1. Ground data

AERONET (<https://aeronet.gsfc.nasa.gov>) provides aerosol optical property data from a sun photometer (e.g., Dubovik et al., 2000; Holben et al., 1998). The standard instrument configuration for AERONET is typically eight wavelengths (340, 380, 440, 500, 675, 870, 1020, and 1640 nm), plus 940 nm for water vapor. Most sites make measurements at approximately 5-min intervals to obtain high temporal resolution data. The estimated uncertainty in AERONET-measured AOD, primarily because of calibration uncertainty, is 0.01–0.02 at an optical air mass of one for network field instruments [with the highest errors in the ultraviolet (UV) region; Eck et al., 1999]. The complete set of Version 3 cloud screening and quality assurance algorithms for AOD data were described by Giles et al. (2019).

The sky radiance was calibrated against frequently characterized integrating spheres at the NASA Goddard Space Flight Center; this measurement was assumed to have an absolute accuracy of ~3% (Sinyuk et al., 2020). Hybrid and almucantar directional scan radiance data were combined with measured AOD data at identical wavelengths as inputs for the retrieval of optically equivalent column-integrated volume size distributions and aerosol refractive indices, using the algorithms developed by Dubovik and King (2000) and Dubovik et al. (2006). These retrieved aerosol properties were used to derive additional parameters, such as the asymmetry parameter, single scattering albedo, and phase function. See Sinyuk et al. (1) for details of the uncertainties in retrieved parameters from sky radiance scans. To ensure sky radiance measurements over a sufficiently wide range of scattering angles, only almucantar scans acquired at a solar zenith angle of $> 50^\circ$ (Level 2) were analyzed in this study. The scattering angle range of measured sky radiances was 100° for an almucantar scan performed at a solar zenith angle of 50° , whereas it was 150° for a solar zenith angle of 75° (Eck et al., 2019).

In this study, level 2.0 and level 1.5 AERONET data were used to compare parameter trends and classify aerosol types, respectively. The level 2.0 data was used to the trend analysis, considering the accuracy of the data. The level 1.5 data were used in an aerosol type classification analysis to obtain a sufficient number of data. In addition, aerosol type classification was only applied to $AOD > 0.4$ to increase data reliability.

Prior to the ground data analysis, we calculated AOD_{550} and fine mode fraction at 550 nm (FMF_{550}) values using an AE of 500 and 675 nm from the AERONET product. This facilitated comparisons between ground and satellite data using the method of previous studies (e.g., Lee et al., 2010). Because the single scattering albedo (SSA) is the ratio of the scattering effect to the extinction efficiency, it was used to examine particle absorption characteristics. The SSA also used to calculate AAOD, AAE, and the scattering Ångström exponent (SAE) in this study. However, SSA can only be identified by an inversion method that uses sky radiance measurements (Dubovik and King, 2000); therefore, the number of data point can differ between the dataset of AOD and those of SSA.

2.2.2. Satellite data

The VIIRS and OMI sensors were launched on the Suomi national polar-orbiting partnership (Suomi-NPP) (Hsu et al., 2019; <https://ncc.nasa.gov/VIIRS>) and Aura satellites (Torres et al., 2013; <https://aura.gsfc.nasa.gov/omi.html>), which have polar-orbit and equator crossing times of 13:30 and 13:45 UTC, respectively. In this study, the

VIIRS/SNPP Deep Blue Aerosol product (AERDB_L2_VIIRS_SNPP), version 1.1, and OMI/Aura Near UV aerosol product (OMAERUV), version 3, were used (Table 1). The sun-synchronous VIIRS sensor provides aerosol data with a spatial resolution of $6 \text{ km} \times 6 \text{ km}$, whereas the sun-synchronous OMI sensor has a spatial resolution of $13 \text{ km} \times 24 \text{ km}$. Because both products are level 2 data controlled by pixel-based results with quality flags, we calculated the daily gridded data through processing using these products. We required at least 500 and 50 satellite retrievals for VIIRS and OMI respectively, in each regional grid (Fig. 1) for a 1-day to ensure that the analysis was valid. For each parameter, the satellite data used in this study were merged according to date for comparison with AERONET daily data.

To examine aerosol trends and classify aerosol types, we used AOD data for a wavelength of 550 nm (AOD_{550}) and AE data collected by the VIIRS sensor, and SSA data for a wavelength of 388 nm (SSA_{388}) and aerosol index (AI) data collected by the OMI sensor. For satellite data analysis, we used AE instead of FMF data, which are not provided over land in the VIIRS product (Hsu et al., 2019). The AE is a qualitative indicator that considers the effect of fine particles in a manner similar to FMF. Therefore, AE was also used as a criterion for aerosol trend and type analyses. SSA data collected by OMI were also used for trend comparisons. The AI data collected by OMI was used for aerosol type classification because the AI is influenced by absorption at UV wavelengths (Ahmad et al., 2006; Torres et al., 2013). Although the OMI data are available from 2004, this study used the data period from 2012 because the VIIRS product is available from March 2012.

2.3. Aerosol type classification

2.3.1. Ground data

Emissions from different sources produce aerosols with different optical properties, allowing their classification into distinct types (Lei et al., 2011; Zhao et al., 2017). Previous studies have developed aerosol classification algorithms for this purpose (e.g., Lee et al., 2010; Omar et al., 2005). Thus, natural and anthropogenic aerosols have been classified according to size (i.e., FMF and AE data) and absorptivity (i.e., SSA and AI data) (e.g., Mok et al., 2017; Ou et al., 2017). Generally, aerosols are classified into three main types: dust (large particles; high absorption in the UV and near UV), BC (small particles; high absorption), and non-absorbing aerosols (small particles; low absorption) (e.g., Higurashi and Nakajima, 2002; Kim et al., 2007; Lee et al., 2010). Aerosols can be further subdivided by modifying these classification methods (e.g., Lee et al., 2010). In this study, the methods used in several previous studies were used to classify aerosol types through the application of aerosol parameters.

The 1.5 level of AERONET data were used for aerosol type classification at ground sites. We limited our analysis of AERONET data to days with $AOD_{440} > 0.4$, in accordance with the methods used in previous studies (e.g., Giles et al., 2012; Lee et al., 2010). However, this approach significantly reduced the amount of data available for analysis; therefore, we added a new aerosol category of 'LOW' when $AOD_{440} < 0.4$. The 'LOW' category increased the temporal continuity of the dataset without significantly affecting the aerosol classification results because the aerosol classification algorithm was only used when AOD_{440} is larger than 0.4 in this study.

For aerosol classification, Cazorla et al. (2013) published a

Table 1
Observation data products and parameters used in this study.

Data	Product	Parameter
AERONET	Daily Average (level 1.5, 2.0)	AOD, AAOD, FMF, SSA, AAE (440, 500, 675, 870 nm)
VIIRS	AERDB_L2_VIIRS_SNPP (v1.1)	AOD_{550} nm, AE
OMI	OMAERUV (v3)	SSA_{388} nm, AI

classification scheme using data from columnar measurements, which is based on AAE and SAE. Cappa et al. (2016) modified the algorithm using in situ measurements. For ground data analysis, we adopted the aerosol classification algorithm of Cappa et al. (2016). Because AAE and SAE also provide absorption characteristics and aerosol size information, we were able to classify aerosol types based on ground observations. Lee et al. (2010) used SSA and FMF, which provide aerosol size and absorbing information, from AERONET to classify aerosol types. Lee et al. (2010) categorized ‘large and high-scattering particles’ as ‘Uncertain’ and ‘small and high-scattering particles’ as ‘NA’.

An example of our aerosol classification results is provided in Fig. 2 for Seoul. For the aerosol classification of ground data, the aerosol classification method proposed by Cappa et al. (2016) was used. In Cappa et al. (2016), large and small particles were divided using the SAE threshold value of 1. The thresholds of $SAE > 1.5$ and $AAE > 2$ indicated fresh smoke aerosols generated from biomass burning, which were more absorbent than BC (Szidat et al., 2007; Singh and Rastogi, 2019). The AAE in the range of 1.5–2.0 and small size aerosols were regarded as a mixture of BC and brown carbon (BrC) (Cappa et al., 2016; Kaskaoutis et al., 2021). This classification was established because the AAE was reduced when it was mixed with other aerosols, either due to aged biomass burning or long-distance transport (Reid et al., 2005; Diapouli et al., 2014). Larger aerosols were classified as $SAE < 1$ and were mixed with dust in the work by Cappa et al. (2016). Low $SAE (< 1)$ and $AAE (< 1)$ aerosols were included in the category with large size and low absorption (Cappa et al., 2016; Kaskaoutis et al., 2021).

We modified the aerosol classes proposed by Cappa et al. (2016), such that the ‘large particle’ class described by Cappa et al. (2016) was renamed as ‘Uncertain’. Furthermore, the ‘small particle and low absorption’ area was renamed to ‘NA’. Thus, aerosols were primarily classified as Dust, BrC, ‘Dust + BC + BrC’, ‘BC + BrC’, ‘Uncertain + BC’, NA, or Uncertain according to the $AAE_{440-870}$ and $SAE_{440-870}$ data obtained from AERONET. The ‘Uncertain’ class means a mixture of BC and large particles from soil dust (Kaskaoutis et al., 2021), but the name was changed to adhere to the method established by Lee et al. (2010).

Because the Cappa et al. (2016) algorithm used several mixed-type categories, we also incorporated the algorithm of Lee et al. (2010), which determines the dominant size mode of aerosols using FMF_{550} data obtained from calculations based on AERONET data. The ‘Dust’ and ‘BC’ types were previously reported to be classified as lower than 0.4 and higher than 0.6 values of FMF_{550} , respectively (Lee et al., 2010). In this AAE–SAE algorithm, the category of ‘Dust + BC + BrC’ was reclassified

into two types based on FMF_{550} threshold of 0.4 (i.e., Dust: $FMF_{550} < 0.4$, BC + BrC: $FMF_{550} > 0.4$). The category of ‘Uncertain + BC’ was reclassified based on FMF_{550} threshold of 0.6 (i.e., Uncertain: $FMF_{550} < 0.6$, BC: $FMF_{550} > 0.6$). FMF values below the threshold were presumed to represent coarse dust particles, whereas values above the threshold were presumed to represent carbonaceous aerosols (CA) from various combustion sources. Lee et al. (2010) defined a ‘mixed type’ class for FMF_{550} between 0.4 and 0.6, but this category was not applied in this study. After this step, the aerosols were classified into seven types using ground data: LOW, Dust, NA, BC, BC + BrC, BrC, and Uncertain.

2.3.2. Satellite data

Several previous studies have proposed aerosol classification methods for use with satellite data (e.g., Kim et al., 2007; Mok et al., 2017). Mok et al. (2017) developed the MOA by modifying the results of studies by Kim et al. (2007) and Lee et al. (2007). The MOA also used the size and absorption information from aerosol optical properties, which was similar to the approach used by Cappa et al. (2016). Therefore, we adopted the MOA for satellite data analysis in this study; however, we substituted VIIRS data for MODIS data and only used land pixels. Accordingly, the 0.95 for AE criterion over land was used as in the MOA (Mok et al., 2017).

The VIIRS–OMI aerosol classification algorithm used in this study is shown in Fig. 3. Before the algorithm was applied, regions within each country were gridded at 1° resolution (i.e., $4^\circ \times 5^\circ$ region was divided into 20 grids). Then, regional average data and aerosol type were assigned to each $1^\circ \times 1^\circ$ grid. For each grid, only cases with data-pixels > 2 (per grid) for AOD_{550} and AE from VIIRS, and data-pixels > 1 (per grid) for AI from OMI were used. The different limits for the number of data points between VIIRS and OMI were based on differences in satellite spatial resolution. This problem was partially resolved through the use of $1^\circ \times 1^\circ$ grids, thereby allowing effective comparison of the data. In addition, grids were removed if all three parameters (AOD_{550} , AE, and AI) were not present together.

After the gridding process, the algorithm estimated the daily data. If only one valid grid was present in a day, the daily aerosol type was classified as ‘undefined’ because of insufficient data. If $AOD_{550} < 0.4$ in all grids, the daily aerosol type was classified as ‘LOW’; this classification process was similar to the process used for the LOW type in ground data analysis for AOD_{440} . Subsequently, if even one of the valid grids had $AOD_{550} > 0.4$, all grids were classified as Dust, NA, CA, Mixture, or Unknown. Based on the AI of 0.8, aerosols with strong absorption were classified as Dust and CA. The AE was also used to separate CA and NA according to absorption characteristics. For example, small AI with high AE indicated low absorbing fine aerosols (i.e., NA). This algorithm was similar to the algorithm from Cappa et al. (2016), which classifies aerosols according to their absorption and size characteristics.

After the aerosol type of each valid grid had been identified, an AOD weighting method was used to determine the daily aerosol type for each region of East Asia. The weighting method used in this study effectively indicated high-impact pollutants and was therefore suitable for our purpose. The aerosol type with the largest total sum of AOD_{550} was regarded as the daily representative aerosol type according to satellite observations. An example of the application for this weighting method for a region of China is shown in Fig. 4. For this date, we defined seven valid grids, each of which was assigned an AOD_{550} value. The sum of these AOD_{550} values (AOD_{sum}) was used to determine the aerosol type. In this example, although NA was the most frequent aerosol type, AOD_{sum} was higher for CA than for NA; therefore, CA was regarded as the daily aerosol type for this date. Consequently, six daily aerosol types were classified using the satellite data: LOW, Dust, NA, CA, Mixture, and Unknown.

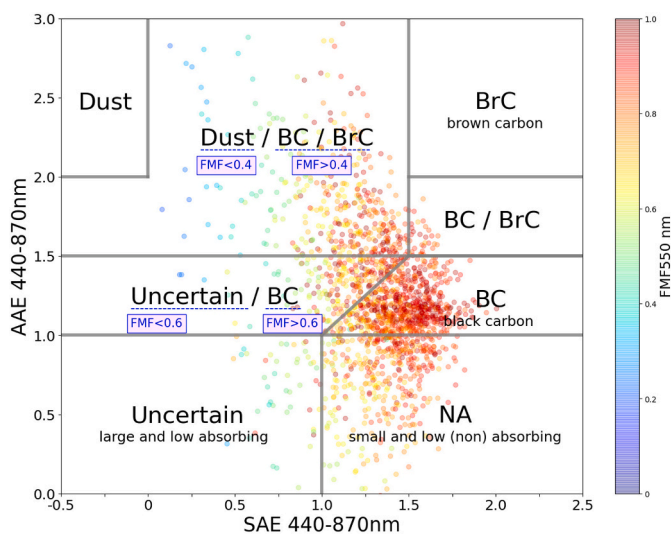


Fig. 2. Example of aerosol type classification based on the AAE–SAE in Seoul. (detailed criteria for aerosol type classification were described by Cappa et al. (2016)).

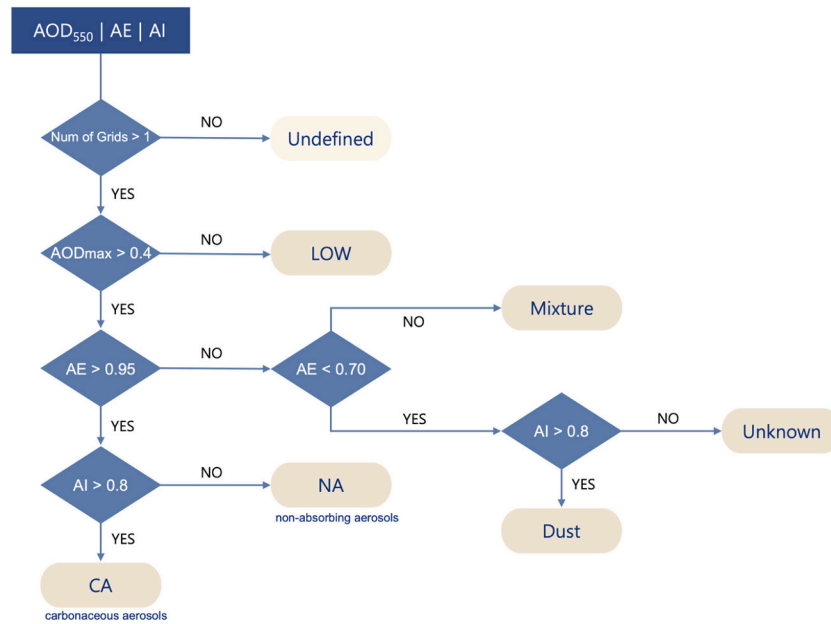


Fig. 3. Flowchart of aerosol type classification using VIIRS and OMI data.

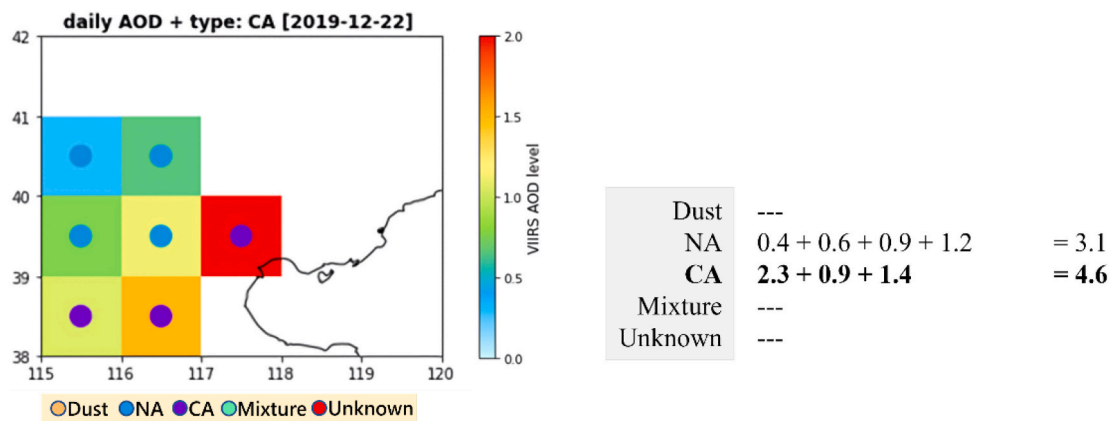


Fig. 4. Example of representative aerosol type determination using the weighting method for VIIRS AOD in China.

3. Results

3.1. Trend analysis

The AOD₅₅₀, FMF₅₅₀, and SSA₄₄₀ from level 2 AERONET data and AOD₅₅₀, AE, and SSA₃₈₈ from VIIRS and OMI data were used in these analyses. Linear regression analysis was performed to identify increasing and decreasing trends in aerosol parameters. Trends in aerosol parameters over the 8-year study period were analyzed based on monthly average data, but the seasonality of AOD was not removed in this study.

The aerosol parameter trends based on ground and satellite data are

shown in Tables 2 and 3, respectively. The slopes and 95% confidence intervals are shown together. For AOD₅₅₀, the slopes of all ground data showed decreasing trends. The rate of AOD₅₅₀ decrease was greatest in Beijing (−0.034 year^{−1}), followed by Seoul (−0.028 year^{−1}) and finally Osaka (−0.003 year^{−1}) site. Of the three ground sites, only the 95% confidence interval of Seoul was negative. The satellite data also showed decreasing trends in AOD₅₅₀ in all three countries (Table 3). The slope of AOD₅₅₀ was highest in China (−0.033 year^{−1}) and lowest in Japan (−0.010 year^{−1}). The AOD₅₅₀ slope was 3-fold higher for China than for Japan. The satellite data also showed that the confidence intervals of AOD₅₅₀ were negative in all countries. The presence of a positive upper

Table 2

Aerosol parameter trends based on ground data. Slope and *p*-values represent aerosol.

Ground	AOD ₅₅₀			FMF ₅₅₀			SSA ₄₄₀		
	Slope	[0.025	0.975]	Slope	[0.025	0.975]	Slope	[0.025	0.975]
Seoul	−0.028	[−0.046	−0.011]	−0.005	[−0.013	0.003]	0.004	[0.001	0.006]
Beijing	−0.034	[−0.080	0.012]	−0.006	[−0.026	0.015]	0.002	[−0.002	0.005]
Osaka	−0.003	[−0.020	0.013]	−0.002	[−0.018	0.014]	0.003	[0.000	0.005]

Parameter trends (AOD₅₅₀, FMF₅₅₀, and SSA₄₄₀) at AERONET sites.

Table 3Aerosol parameter trends based on satellite data. Slope and p-values represent aerosol parameter trends (AOD₅₅₀, AE, and SSA₃₈₈) in the three countries.

Satellite	AOD ₅₅₀			AE			SSA ₃₈₈		
	Slope	[0.025	0.975]	Slope	[0.025	0.975]	Slope	[0.025	0.975]
Korea	−0.014	[−0.024	−0.005]	−0.015	[−0.024	−0.006]	−0.002	[−0.003	0.000]
China	−0.033	[−0.045	−0.021]	−0.012	[−0.027	0.003]	−0.033	[−0.045	−0.021]
Japan	−0.010	[−0.017	−0.003]	−0.020	[−0.031	−0.010]	−0.010	[−0.017	−0.003]

limit only for Beijing and Osaka may be the result of insufficient data points, as shown in Fig. 5b and c. In summary, clear decreasing trends in AOD₅₅₀ were observed in all three countries, according to both satellite and ground data. The confidence intervals for all country regions were negative; therefore, the reliability of the decreasing trend was higher at the country level than at the ground site level. In a previous study using AERONET, Beijing and Osaka showed −0.10 and −0.06 decadal trends in AOD, respectively (Li et al., 2014); although the previous findings slightly differed from our results, there was a clear decrease in AOD. Furthermore, fine dust levels in the atmosphere have steadily increased since industrialization, but PM_{2.5} has been decreasing in East Asia, especially since 2010 (Yin, 2021). In China, PM_{2.5} levels tended to significantly decrease (approximately 30–50% of the total) between 2013 and 2018 (Zhai et al., 2019). Furthermore, according to the Seoul Institute Health (2021) the PM_{2.5} concentration in Seoul significantly decreased from 2007 to 2020. Similarly, Ho et al. (2021) suggested that the decreased air pollution levels in Seoul in the 2010s may have resulted from regulatory requirements concerning vehicle emissions in Korea, which have been in effect since 2005. Lee et al. (2018) found that the Clean Air Act has led reduced air pollution, with a 9% decrease in PM₁₀ levels between 2003 and 2006. AOD and particulate matter (PM) are very closely related, and the decrease in AOD indicated that the occurrence of high concentrations of pollutants continuously decreased at all sites covered by ground and satellite observations.

FMF₅₅₀ showed decreasing trends at all ground sites (Table 2), with the range of −0.005 year^{−1} (Seoul) to −0.002 year^{−1} (Osaka). Seoul and Beijing had decreasing trends of −0.005 year^{−1} and −0.006 year^{−1}, but the confidence interval of Seoul [−0.013–0.003] was much narrower than those of Beijing [−0.026–0.015]. Satellite data were analyzed in terms of AE instead of FMF, and also showed decreasing trends in all countries, with the greatest decrease occurring in Japan (−0.020 year^{−1}) and the lowest in China (−0.012 year^{−1}). Decreases in FMF and AE indicate a decreasing amount of small particle. A previous study suggested that the decreasing FMF in northeast China is associated with a decrease in anthropogenic activities because of the regulations imposed by clean air policies (Yan et al., 2022). In contrast to the present study, Yan et al. (2022) used a deep learning approach, which revealed that India and the western USA had strong increasing trends in FMF (> +0.003 year^{−1}) (Yan et al., 2022). In summary, the influence of fine particles continuously decreased at all observation points throughout East Asia because of the decrease in anthropogenic pollution. There were similar FMF and AE slope directions for all three countries, but the level of significance differed among countries. With respect to AOD and size parameters (FMF₅₅₀ and AE), the trends from ground-based observations were statistically insignificant, although the trends from satellite and ground observation generally showed the same tendencies. The weak significance level from the ground-based data was caused by temporal data inhomogeneity due to the limitation of the observation

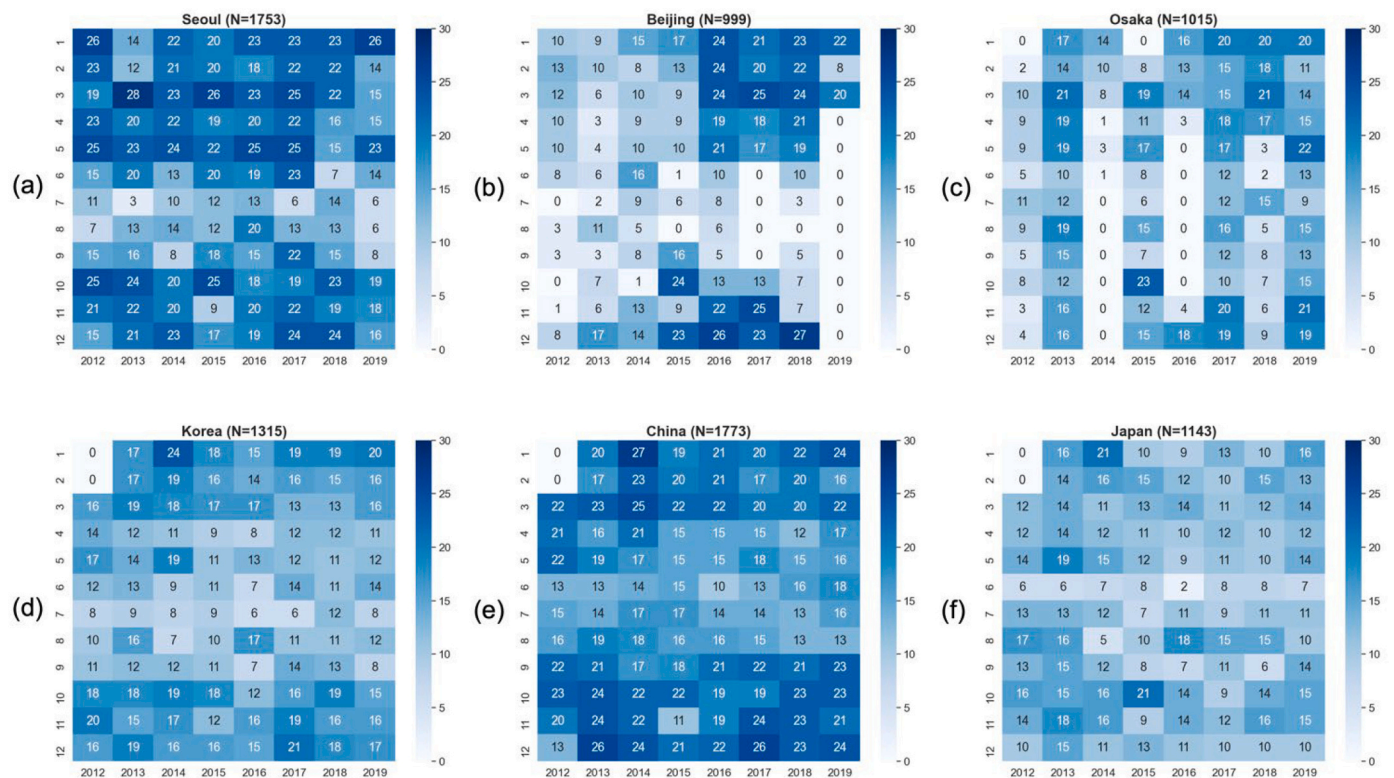


Fig. 5. Monthly distribution of valid observations for the daily aerosol type classification in (a) Seoul, (b) Beijing, and (c) Osaka from AERONET, and (d) Korea, (e) China, and (f) Japan from satellite observations.

conditions.

The AERONET SSA₄₄₀ slopes slightly differed from the other parameter trends, as shown in Table 2, with slight increases in SSA₄₄₀ at all ground sites. In Beijing, the SSA₄₄₀ trend was 0.002 year⁻¹, and its 95% confidence interval had negative values, unlike the other sites. However, the OMI SSA₃₈₈ slopes indicated decreasing trends in all countries (Table 3). The SSA₃₈₈ results in China and Japan were less reliable than the results from ground sites. The SSA is the scattering ratio of light extinction; therefore, a decreasing SSA can be caused by increasing levels of high-absorbing aerosols or decreasing levels of low-absorbing aerosols. Eck et al. (2013) suggested that the increasing SSA over 15 years in the southern African biomass-burning region could be the result of a decrease in the BC fraction. Therefore, the trends in SSA could also be caused by a decrease in anthropogenic pollution. The SSA results suggested that pollution had decreased over a larger area than the area covered by the ground sites. However, the significance levels for the trends from satellite and ground observations were statistically insignificant in all cases.

Consequently, the trend analysis indicated that the satellite data

were consistent overall, with decreasing trends in AOD₅₅₀, FMF₅₅₀, and AE in all regions. The trends from the ground data also showed a negative slope compared with the trends from satellite data, although the significance level was slightly weaker. Decreases in FMF and AE could be related to the decrease in anthropogenic activities caused by air-quality regulations. This FMF result was similar to the trend previously described in East Asia, but it slightly differed from the trends that have been observed in the USA and India (e.g., Yan et al., 2022). A decreasing SSA could be related to an increase/decrease in high/low-absorbing particles, as well as a decrease in pollution. Given the pollution levels and particle size data obtained in this study, we concluded that these consistent trends were the result of significant reductions in fine particle levels.

3.2. Aerosol types

3.2.1. Annual variation

To determine the causes of the observed parameter trends, we examined temporal variation in the dominant aerosol types over time,

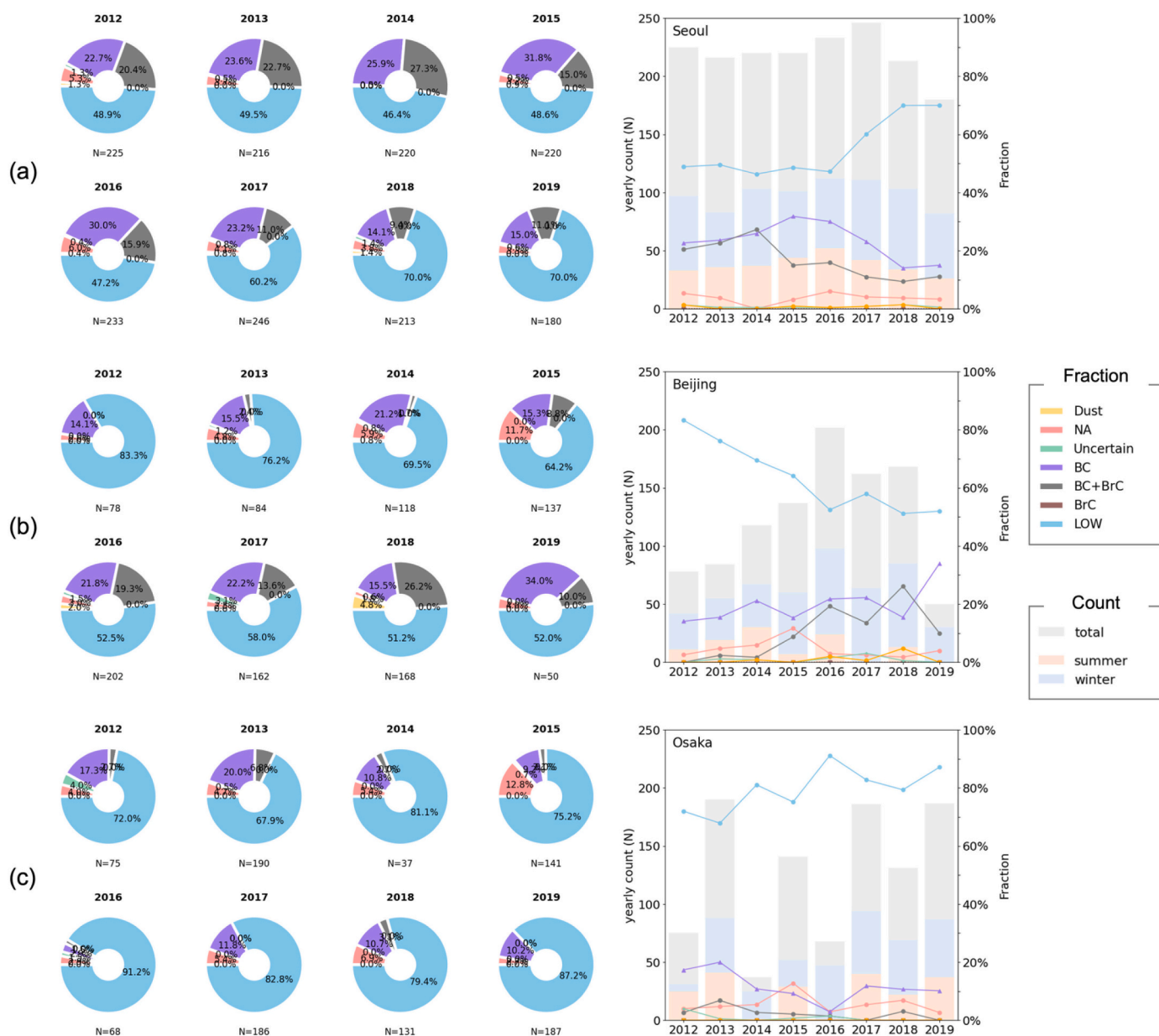


Fig. 6. Annual frequencies of aerosol types (pie charts) during 2012–2019 based on ground observations in (a) Seoul, (b) Beijing, and (c) Osaka.

which was related to aerosol optical properties (e.g., [Ou et al., 2017](#)). [Fig. 5](#) shows the valid number of observations for the classification of aerosol type. Based on the observation frequency shown in [Fig. 5](#), the annual frequency results for aerosol types during 2012–2019 based on ground and satellite data are shown in [Figs. 6 and 7](#), respectively. Seven aerosol types (i.e., LOW [$\text{AOD}_{440} < 0.4$], Dust, NA, BC, BC + BrC, BrC, and Uncertain) are shown in [Fig. 6](#). For ground data, we noted that the annual variation in the number of data points was inconsistent. The irregularity of ground data is clearly visible in [Fig. 5](#). For the simultaneous consideration of seasonal variation in aerosol type dominance, the bar chart in [Fig. 6](#) also shows data counts for summer and winter. There were no data corresponding to the BrC category in our results.

In Seoul, the LOW fraction increased from 2016 ([Fig. 6a](#)); this involved a significant increase from 47.2% (2016) to 70.0% (2019), compared with the previous period (2012–2015). Similarly, [Cho et al. \(2021\)](#) reported that years with smaller than 0.4 for a mean MODIS AOD significantly increased after 2014 in the Korean Peninsula. From 2015 to 2018, the BC fraction decreased from 31.8% to 14.1% and the BC + BrC fraction decreased from 15.0% to 11.1% in Seoul ([Fig. 6a](#)). The NA

fraction was less variable than the fractions of all other aerosol types ([Fig. 6a](#)). At Yonsei University site, [Lee et al. \(2018a, 2018b\)](#) found fractions of approximately 20% for NA and >60% for BC in the summer of 2015, using a previously developed method from [Lee et al. \(2010\)](#). However, the values in the present study were considerably different (NA: 2.2%, BC: 31.8%, BC + BrC: 15.0%, and LOW: 48.6%). Because [Lee et al. \(2010\)](#) required SSA and FMF, the differences could be related to the method used for type classification. In Anmyeon, Korea, [Choi et al. \(2016\)](#) found a 70% BC + Dust + organic carbon fraction among cases with an AOD_{440} of >0.4 during 1999–2007. Therefore, a large ratio of BC to BC + BrC is not unusual. The Dust fraction was rarely observed, but a value was obtained for some years ([Fig. 6a](#)). Consequently, there was significant variation in the dominant aerosol type frequency in Seoul from 2015 onward. The proportions of the LOW, BC, and BC + BrC aerosol type were more variable than the proportions of all other types.

The fraction of LOW in Beijing continuously decreased throughout the study period, from 83.3% (2012) to 52.0% (2019) ([Fig. 6b](#)). [Li \(2020\)](#) reported that the AERONET AOD showed a decreasing trend from 2008 until 2016 in Beijing. Trend analysis in the present study also

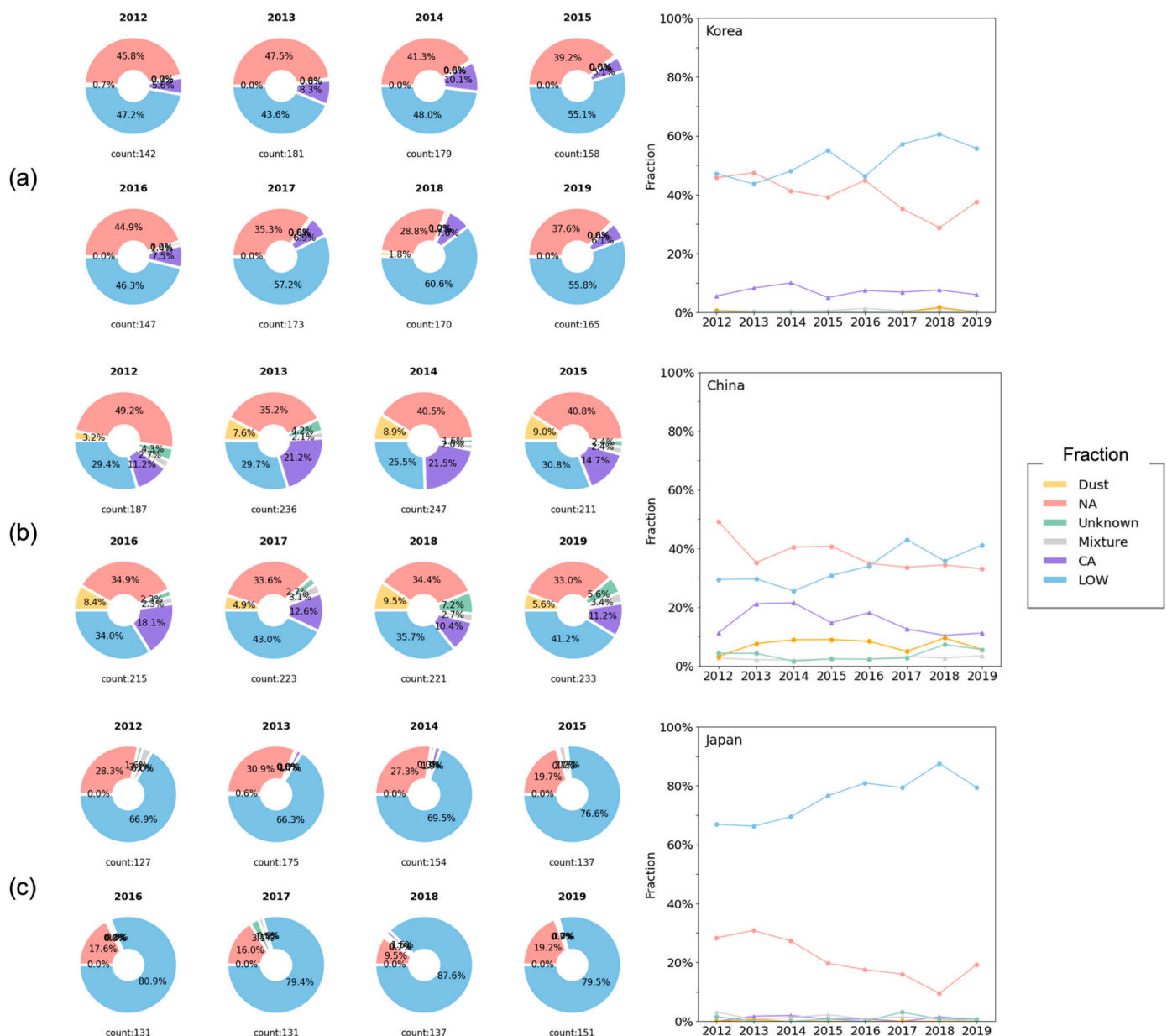


Fig. 7. Annual frequencies of aerosol types (pie charts) during 2012–2019 based on satellite observations in (a) Korea, (b) China, and (c) Japan.

showed a decreasing slope for Beijing. In a previous study, in the Daxinganling, region of China, a decreasing MODIS AOD was apparent from 2000, when the lowest AOD was observed (Guo et al., 2011). Therefore, the decreasing LOW fraction during periods with a decreasing AOD₅₅₀ may not be the result of increasing pollution, this decreasing fraction may be related to the greater impact of the decrease in high AOD values, compared with the impact of the increase in low AOD. In contrast, the fractions of BC and BrC increased, with significant fluctuation observed in Beijing. The fraction of BC + BrC significantly increased from 2.4% (2013) to 26.2% (2018), whereas the fraction of BC slightly increased from 14.1% (2012) to 34.0% (2019). The fraction of Dust was nearly 2-fold higher in Beijing than in Seoul (Fig. 6a) in certain years. Beijing had the largest fraction of Dust (4.8%) in 2018; however, its annual average fraction of Dust was <3% (i.e., an insignificant proportion) and annual variation was very low. The fraction of NA was lower than 10% in Beijing. Ou et al. (2017) discovered that the fraction of ‘scattering type’ aerosols was 15–20% in 2012–2015 period. In this study, the NA fraction in cases with AOD₄₄₀ > 0.4 ranged from 15.6% (2012) to 32.7% (2015). The fraction of BC was high especially in 2019, which may be related to a lack of data. Consequently, the fraction of LOW type significantly decreased throughout the study period, whereas the fraction of BC + BrC increased significantly. Similarly, Ou et al. (2017) showed that the ‘moderately-absorbing type’ and ‘highly-absorbing type’ in Beijing increased continuously from 2012, which may explain our result as increasing BC + BrC fraction in the present study. Using the Modern-Era Retrospective analysis for Research and Applications (MERRA), Provencal et al. (2017) revealed a strong increasing trend in the AOD of BC in Beijing (over 0.0005 year⁻¹ during 2003–2015). However, Dehkoda et al. (1) showed that the AAOD of BC continuously decreased from 2002 to 2017. Therefore, our results indicate that although the fraction of BC category increased, the absorption characteristics of the aerosol decreased.

The fraction of LOW in Osaka increased from 72.0% (2012) to 87.2% (2019) (Fig. 6c), which was the largest proportional increase among all sites. The higher fraction of LOW in 2014 and 2016 was related to a lack of data in summer (Fig. 5c). The fraction of BC + BrC type was nearly halved from 6.8% (2013) to 3.1% (2018) (Fig. 6c), although BC + BrC was only observed annually for 2 years from 2016. Dehkoda et al. (1) found that the AAOD of BC continuously decreased from 2002 to 2018 in Osaka, which could explain the decreasing BC + BrC trend observed in this study. In Osaka, the mean fraction of NA aerosols was approximately 5% excluding 2015. The fraction of BC was approximately 10% when averaged across the study period. In Osaka, the BC fraction reached 20.0% in 2013 and 10.2% in 2019. The fraction of Dust was not observed during this period. Similarly, Shao and Dong (2006) reported that the mean dust concentration from 1998 to 2003 was near zero in Japan. Consequently, with the exception of the LOW and BC + BrC fractions, we observed no continuous increases or decreases among the aerosol types.

In summary, changes in the LOW, BC, and BC + BrC fractions were observed from 2012 to 2019 at most ground sites, whereas consistent changes were not detected among the other aerosol types. In Seoul, we observed increases in the LOW fraction and decreases in the BC and BC + BrC fractions. In Beijing, the LOW fraction significantly decreased, whereas the BC + BrC fraction increased. In Osaka, the LOW and BC + BrC fractions increased and decreased, respectively. The highest Dust fraction was detected in Beijing, whereas Osaka was not significantly affected by Dust. In 2018, the highest Dust fractions were observed in Seoul and Beijing (4.8%). The variation among sites may have been related to regional differences. Some similarities in dominant aerosol types over time were also observed.

The trends in annual aerosol type and aerosol optical properties were considered concurrently. AERONET AOD₅₅₀ values significantly decreased over time at all ground sites. The decreasing trends may have affected the observed increasing LOW fraction, which had a low AERONET AOD₄₄₀ value. The decreasing trend in AOD could also be related

to the decrease in the number of high AOD cases, rather than an increase in the number of low AOD cases. The decreases in AERONET AOD₅₅₀ and FMF₅₅₀ could also be interpreted as a decrease in the high concentrations of fine particles at the ground sites. The BC + BrC fraction was reduced at two of the three ground sites (Seoul and Osaka). These results suggest a decreasing effect of high-absorbing aerosol concentrations at these two sites. The decreasing BC + BrC fraction could increase the SSA values. Choi et al. (1) showed that sites with a high concentration of CA had a low SSA in Korea. Thus, the BC + BrC trends observed at the Seoul and Osaka sites could explain the increasing SSA₄₄₀ trend. Although there was an increase in the BC fraction, the decrease in the AAOD of BC may be related to the increasing SSA value in Beijing.

Using satellite data, we identified annual changes in aerosol type patterns over larger areas. For the satellite data, six aerosol types were analyzed using the VIIRS-OMI algorithm: LOW (maximum value of AOD at 550 nm is <0.4), Dust, NA, CA, Mixture, and Unknown aerosols (Fig. 7). The temporal variation in size was more homogeneous for satellite data than for ground data (Fig. 5d–f), and therefore the amount of annual data is not indicated in Fig. 7.

The fraction of NA aerosols in Korea gradually decreased from 45.8% (2012) to 37.6% (2019) (Fig. 7a), and the fraction of LOW increased from 47.2% (2012) to 55.8% (2019). The increasing in the fraction of LOW was similar to the increase observed at ground sites (Fig. 6a), and Cho et al. (2021) reported a decreasing AOD in the Korean Peninsula. All other aerosol types displayed minimal annual variation, with the exception of LOW and NA fractions. In Korea, CA constituted approximately 8% of all aerosols throughout the study period, with the highest value in 2014 (10.1%). Seoul had the highest CA fraction, with the sum of BC and BC + BrC comprising 53.2% of the total aerosols in 2014 (Fig. 6a); the CA fraction in Korea was also highest in 2014 (Fig. 7a). It was difficult to identify a continuous increase or decrease in CA in Korea. The Dust, Mixture, and Unknown fractions constituted <1%, indicating a very weak influence. There were only noticeable changes for the LOW and NA fractions. In contrast to the results for ground sites, the NA fraction was very high and the CA fraction was very low. The NA fraction was between 73.1% (2018) and 84.2% (2013) for cases with an AOD₄₄₀ > 0.4. Similarly, Kim et al. (2007) showed that the “sulfate type” calculated from the satellite algorithm (MOA) had a frequency of >60% in the East Asia region. The slight gap in CA in both ground and satellite data could be the result of low BC sensitivity. Because BC is mostly present near the surface, its low AOD leads to poor detection by satellite sensors (Ramachandran et al., 2020).

In China, the NA fraction continuously decreased from 49.2% (2012) to 33.0% (2019), whereas the LOW fraction increased from 29.4% (2012) to 41.2% (2019) (Fig. 7b). With the decreasing AOD in China, the LOW fraction continuously increased; however, the Beijing site data differed from the data describing China overall. The CA fraction was approximately 10% higher in China than in Korea. Using MERRA AOD data, Provencal et al. (2017) found that the mean BC fraction constituted approximately one-sixth of all aerosols, which was similar to our result of approximately one-fifth. The mean NA fraction from the MERRA AOD data was approximately 60% (Provencal et al., 2017), which was similar to our NA result in cases where the AOD₄₄₀ was larger than 0.4. The CA fraction decreased in China from 2014, whereas the BC + BrC fraction at the Beijing site tended to increase during the same period. The decrease in the CA fraction in China since 2013 may be a result of the “Clean Air Action” program that was implemented in 2013 to 2017. The Clean Air Action program launched stringent measures to achieve higher air-quality targets, including adjustments of energy production and industrial structures, as well as reductions of air pollutant emissions (China State Council, 2013). As a result of the program, the consumption of coal and hydrocarbon fuels in China decreased after 2013 (Zheng et al., 2018). This decrease in hydrocarbon emissions could explain the decreasing CA fraction in Fig. 7b. The differences between Beijing and China overall may be related to differences between urban and suburban

areas. Dingenen et al. (2004) reported that urban and rural area showed significant differences in PM concentration and particle size. Nguyen et al. (2019) reported substantial differences in AOD between urban and rural aerosols. The Dust fraction in China was <10% annually, and the highest fraction occurred in 2018 (9.5%). Provencal et al. (2017) reported that the fraction of mineral dust was similar to the fraction of BC, but we found that the Dust fraction was half of the CA fraction. All other aerosol types constituted <10%, with minimal annual variation. Thus, we observed continuous increases and decreases in the NA, LOW, and CA fractions in China.

In Japan, the fraction of NA substantially decreased from 28.3% (2012) to 19.2% (2019), whereas the fraction of LOW increased from 66.9% (2012) to 79.5% (2019) (Fig. 7c). The fraction of LOW was the highest of the three sites; this high fraction was related to the low mean AOD in Japan, as described by Xia et al. (2016). Consistent with the result in this study, other studies during this period have shown that the AOD in Osaka decreased (e.g., Provencal et al., 2017); the AOD also decreased in other sites in Japan (e.g., Wang et al., 2021). The proportions of all other aerosol types were < 4%, with minimal variation. The annual CA fraction was similar to the fractions of the Mixture and Unknown aerosol types. Pollutant emissions in Japan have decreased since the 1970s because of air-quality regulations (Kurokawa and Ohara, 2020). The total annual amount of SO₂, NO₂, and BC emitted in Japan was <0.3 Tg in the 2010s (Kurokawa and Ohara, 2020), but in China it was >3 Tg per year in the 2010s (i.e., 10-fold higher than in Japan; Kurokawa and Ohara, 2020). This may explain the significantly lower fractions of CA and other aerosol types in Japan (Fig. 7c). The Dust fraction was not observed in Japan throughout the study period, which was consistent with the ground observations (Fig. 6c). Therefore, increasing and decreasing trends in the NA and LOW fractions, respectively, were noticeable in Japan, whereas there were no significant trends in the other aerosol types.

According to the annual variation in the dominant aerosol types derived from satellite data, the NA fraction significantly decreased in all countries, whereas the LOW fraction substantially increased. The mean LOW fraction was highest in the order of Japan, Korea, and China, whereas the opposite pattern was observed for the CA fraction. The CA fraction also showed a constant decline in China. The fractions of all other aerosol types did not significantly change over time in any country.

Considering the aerosol type and optical property results, the increasing LOW fraction was related to the decreasing trend in AOD₅₅₀ in all countries. The decreases in AOD₅₅₀ and AE in all countries could be interpreted as an indication of the reduced effect of high concentrations of fine particles. Along with the decreasing AOD in our results, there was also a long-term decrease in fine mode AOD confirmed during 2012–2019 in Japan, with a rate of decline of $-2.7 \pm 1.1\%$ year⁻¹ (Itahashi et al., 2021). The reductions in AOD₅₅₀, AE, and NA fraction occurred simultaneously, and the effect of high NA aerosol concentrations was reduced in all countries. In China, the CA fraction continuously decreased along with the fraction of NA aerosols from 2014 to 2019 (NA, 40.5% to 33.0%; CA, 21.5% to 11.2%).

The decline in NA fraction in all countries may be related to changes in emission characteristics over time. As environmental concerns have increased, there has been increasing regulation of industrial activities and air pollution worldwide; coal consumption has also decreased in recent years (Dudley, 2018). In many countries, SO₂ emissions have continuously decreased (Smith et al., 2001; Zhong et al., 2020). For example, China established the 10th and 11th five-year plans, and these regulations achieved SO₂ emission reductions (Schreifels et al., 2012; Ronald et al., 2017). In east China, the OMI SO₂ trend was below -0.25 Dobson units/decade during 2005–2017 (Li, 2020). In the Yellow Sea between Korea and China, the amount of SO₂ emitted significantly decreased from 2012 onward (~ 30 Tg/yr) to 2017 (~ 10 Tg/yr) (Itahashi et al., 2021). Zheng et al. (2018) showed that SO₂ emissions significantly decreased from 2011 (~ 30 Tg) to 2017 (~ 10 Tg), which

could be a result of the Clean Air Act in China. SO₂ can be converted to particulate sulfate through oxidation (Gen et al., 2019). Sulfate is regarded as an NA aerosol because of its weak absorption properties, according to optical-based type classification. Therefore, a decrease in SO₂ emissions could lead to a decline in NA fraction.

To summarize the annual dominant aerosol results, changes in the LOW and CA fractions were observed in ground data, whereas changes in the LOW and NA fractions were observed in satellite data. The CA fractions at the study sites increased in the order of China, Korea, and Japan, whereas the opposite pattern was observed for LOW aerosols. The annual maximum CA fraction occurred in Korea (Seoul). The decreasing trend in CA after 2013 could be a result of air pollution control policies in China. Changes in the dominant aerosol type could explain the increasing and decreasing trends observed in most aerosol optical properties. In particular, the decreasing NA fraction in all countries could be a result of decreasing SO₂ levels, which were likely caused by the enhanced regulation of air pollution emissions (e.g., the Clean Air Act in China). Most of the data are consistent with the results of previous studies. China and Beijing had different trends in terms of dominant aerosol types, which could be explained by differences between urban and suburban areas.

3.2.2. Seasonal characteristics

For a given region, the dominant aerosol type differs seasonally according to aerosol emissions characteristics and transport patterns (Kedia et al., 2014). For this reason, seasonal inhomogeneity in the amount of data used can lead to bias in analyses of annual aerosol types. Therefore, we additionally analyzed the dominant aerosol types in the study regions according to ground and satellite data at the seasonal scale (Figs. 8 and 9). The study period was divided into spring, summer, fall, and winter. The seasonal frequency distribution of aerosol types according to ground data are shown in Fig. 8. There were no data corresponding to the BrC category in our results.

At the Seoul site, the LOW fraction was >70% in fall and winter; it was lowest in summer (35.2%) (Fig. 8a). The seasonal BC and NA fractions were highest in summer; however, the seasonal variation in NA aerosols was $\pm 5\%$. The BC + BrC fraction was higher in spring than in the other seasons. The BC fraction was 43.4% in summer. The low LOW fraction could be related to the high AOD in summer. Zhai et al. (2021) reported that the geosynchronous equatorial orbit satellite AOD in South Korea was high in the spring and summer of 2016. Many previous studies showed that the mean AOD was usually higher in summer than in other seasons within the East Asia region (e.g., Eck et al., 2005; Lee et al., 2007; Choi et al., 2016). Choi et al. (2016) found that the highest fractions of low AOD (<0.4) aerosols were present in June and July in Anmyeon, Korea during 1999–2007. The Dust fraction was <2% in spring and < 1% in winter (Fig. 8a). Similarly, Shin et al. (2019) found that the Dust fraction-dominated mixture in Seoul was highest in spring. The BC and BC + BrC fractions displayed different seasonal characteristics. In a previous study, the BC mass density at Yonsei University was highest in spring and winter during 2011–2018 (Choi et al., 2020), which could explain why our study identified the highest BC + BrC fraction in spring. Compared with the characteristics of BC + BrC, the characteristics of BC were more similar to the distribution tendency of NA. The NA fraction was highest in summer, which was similar to the findings by Shin et al. (2019), although the frequency of occurrence was different. In our study, the NA fraction in summer was 10.2% in cases where the AOD was >0.4 (Fig. 8a), but Shin et al. (2019) found that the mean occurrence in summer was approximately 50% in Seoul. Lee et al. (2018a, 2018b) found that the NA fraction was approximately 20% in Yonsei University during May and June of 2015. This discrepancy could be related to differences in the algorithms used. Because NA and BC are classified based on their absorption characteristics when using an optical algorithm, the aerosol type can change depending on the threshold. This characteristic could explain why the BC distribution was similar to the NA distribution, rather than the BC + BrC distribution.

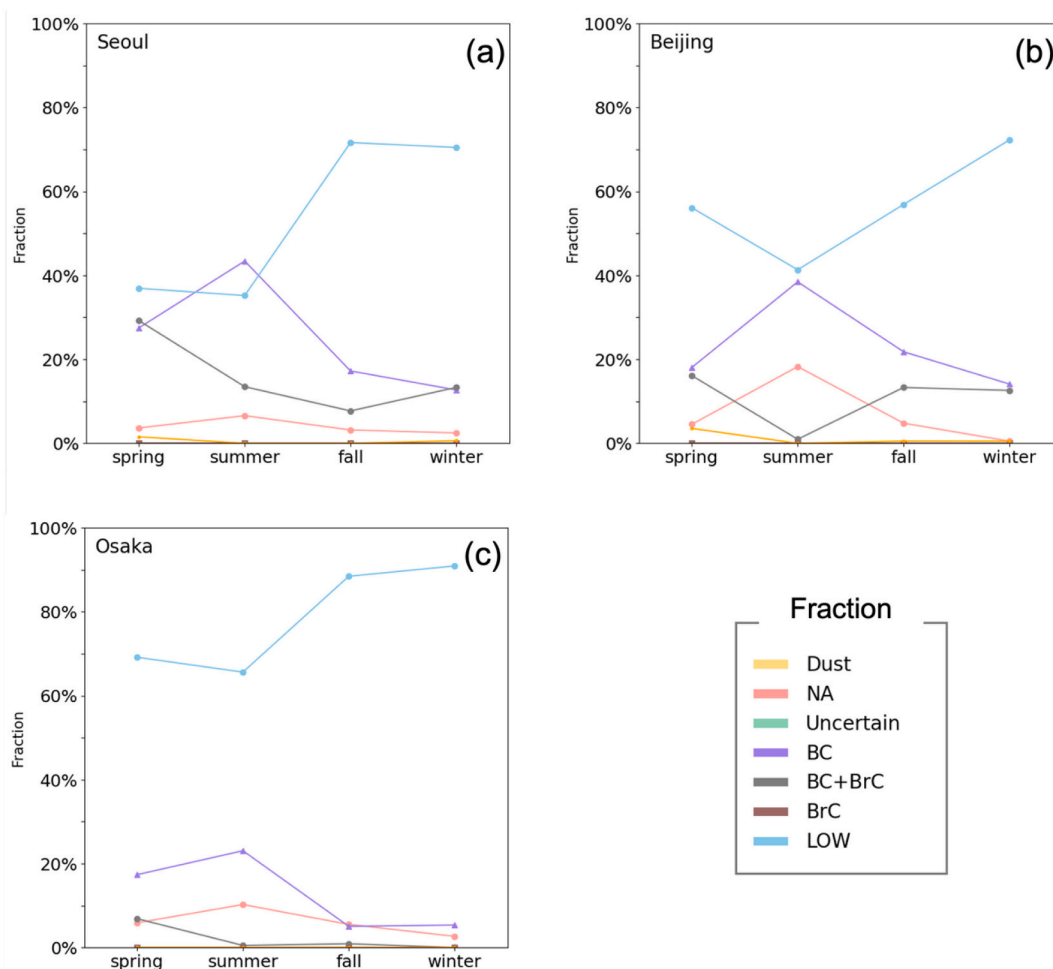


Fig. 8. Seasonal frequency distribution of aerosol types according to ground observations in (a) Seoul, (b) Beijing, and (c) Osaka.

In Beijing, the LOW fraction was 40–75% in all seasons (Fig. 8b). The LOW fraction was the most common aerosol type in winter (72.2%); it was similar in spring (56.1%) and fall (56.9%). The lowest LOW fraction occurred in summer in the North China Plain; moreover, AERONET AOD and MERRA-2 AOD were highest in June for approximately 10 years before 2014 (Song et al., 2018). In summer, the BC fraction was highest in Beijing (38.5%). Large differences were observed in the NA and BC + BrC fractions between summer and winter. The seasonal difference in NA frequency was approximately 20%, which was approximately twofold greater than the seasonal difference at the Korea and Japan sites. In fall and winter, the BC + BrC fraction was approximately 15% (Fig. 8b), but it was nearly absent in summer. Similarly, the mean equivalent BC in Beijing was reportedly high in winter from 2012 to 2020 (Sun et al., 2022). Choi et al. (1) found that the overall BC mass density, including Beijing and several sites in Korea, had a lower value in summer; this explained the low BC + BrC fraction in summer. A previous study revealed that the frequency of scattering fine-type aerosols was highest in August and September in Beijing (Zhang and Li, 2019), which was similar to our result for the NA fraction in summer. The BC fraction was also high in summer, which could be the result of algorithm-based adjustment of scattering and absorbing aerosols, as mentioned earlier. The Dust fraction reached a maximum of 3.5% in spring (Fig. 8b). Similarly, Zhang and Li (2019) discovered that dust desert aerosols constituted a large fraction in spring. Shin et al. (2019) found that dust dominated the aerosol mixture in spring, and the pure dust fraction was approximately 20% in spring during 2001–2017. This was slightly different from our result in Beijing (8.0% Dust fraction in spring for cases of AOD > 0.4). Yu et al. (2017) found that the fine mode AOD was

highest in summer and the coarse mode AOD was highest in spring, which could explain our results for the Dust fraction in winter and NA and BC fractions in summer.

The LOW fraction was more frequently observed in Osaka than at other sites (Fig. 8c). Osaka was cleanest in winter, with levels of the LOW fraction reaching 90.9%. The LOW fraction was lowest in summer. Similarly, the mean AOD₄₄₀ in Osaka was highest in summer (0.64 ± 0.21) during 2001–2018 (Dehkhoda et al., 2020). The BC fraction was highest in summer (23.1%), although this was approximately 15% lower than the levels at all other sites. The NA fraction was 10.3% in summer (Fig. 8c). A previous study showed that the fine mode AOD was high in summer during most years from 2001 to 2020 in the Seto Inland Sea region of Japan (Itahashi et al., 2021). Osaka also had an NA fraction of almost 40% in July and August during 2000–2016 (Shin et al., 2019). The highest BC + BrC fraction was 6.9%, indicating that this fraction was not dominant in Osaka (Fig. 8c). Similar to our results, Dehkhoda et al. (1) found that the mean AAOD of BC was more than threefold lower in Osaka than in Beijing.

At all ground sites, the LOW fraction was highest in winter or fall and lowest in summer. This was consistent with the results of many previous studies, in which the mean AOD in East Asia was generally higher in summer (e.g., Eck et al., 2005; Lee et al., 2007; Choi et al., 2016). The characteristics of the BC fraction differed from the characteristics of the BC + BrC fraction in all seasons, although both fractions are types of CA. Notably, BC had the greatest effect in summer at all ground sites, which was similar to the seasonal variation observed in NA aerosols. This characteristic was related to differences in the algorithms used, as mentioned earlier. The Dust fraction was highest in spring in Beijing and

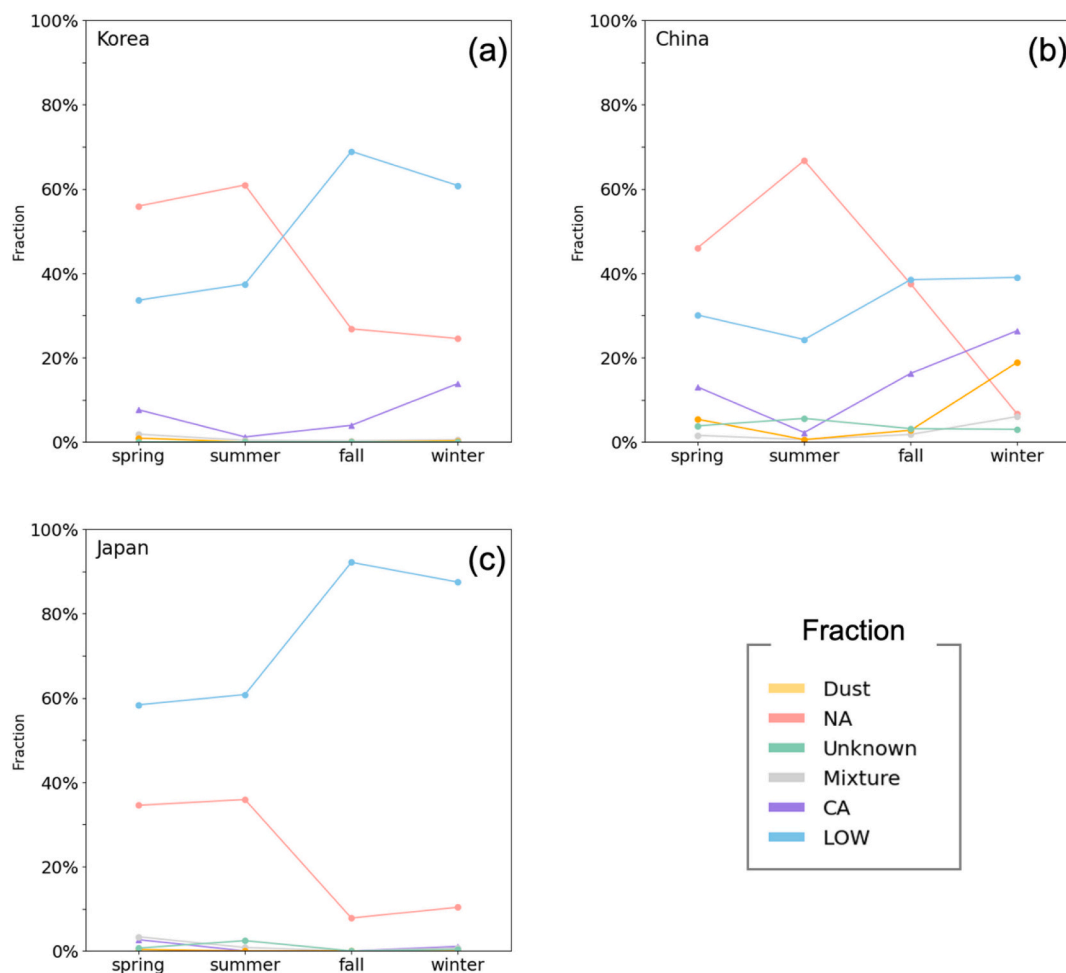


Fig. 9. Seasonal frequency distribution of aerosol types according to satellite data in (a) Korea, (b) China, and (c) Japan.

Seoul, whereas no Dust was detected in Osaka. Thus, seasonal similarities and differences were detected at all three sites.

Short-term variation in the frequencies of the different aerosol types were partially affected by the seasonal and annual inhomogeneity in the amount of data. The high frequency of the LOW fraction in 2014 and 2016 could be related to the lack of summer data in Osaka (Figs. 5c and 6c). We identified Beijing's maximum BC and minimum LOW in 2019, despite the lack of summer data (Figs. 5b and 6b). This inconsistency may be driven by insufficient annual data numbers.

The seasonal aerosol type patterns derived from satellite data are shown in Fig. 9. In Korea, the LOW fraction reached >60% in fall and winter (Fig. 9a). Similar to the ground data (Fig. 8a), the highest LOW fraction was observed in fall (68.9%) in Korea. Another study showed that the mean AOD in South Korea is low in fall and winter (Zhai et al., 2021). The MODIS AOD₅₅₀ in the large area surrounding Korea was very low, <0.35 from September to December during 2004–2014, which may explain the high fraction of LOW in fall. The fraction of NA aerosols was >55% in spring and summer, whereas it was approximately <10% according to ground data (Fig. 8a). As mentioned earlier, the differences between region/country data and ground-site data could be related to the algorithm used (e.g., differences in NA fraction between Kim et al., 2007 and Lee et al., 2018a, 2018b). According to the satellite data for Korea, the CA fraction was 13.8% in winter and < 2% in summer. Other aerosol types were rarely observed. The CA fraction in Korea was highest in winter, and the high CA in winter may have influenced the LOW fraction. Lee et al. (2021) reported that most AERONET sites in Korea had a low mean SSA₄₄₀ in winter, which could be explained by our results regarding the CA fraction in Korea.

In China, the fraction of LOW was approximately 20–40% (Fig. 9b), which was approximately 20% lower on average for each season, compared with the fraction of LOW derived from ground data (Fig. 8b). The low fraction of LOW could be related to the high mean AOD in China. Liu et al. (2021) found that the Beijing-Tianjin-Hebei region of China had the highest MODIS AOD in summer during 2007–2020, which was similar to our finding of the low fraction of LOW in summer. The fraction of NA aerosols was 66.8% in summer and 6.6% in winter, indicating a large difference between seasons. The shape of the line plotted for the NA fraction was similar to the result in Beijing (Fig. 8b), but the seasonal difference in China was 3-fold greater than in Beijing. The fraction of CA was lowest (< 3%) in summer and highest (26.4%) in winter. The CA fractions were similar between spring and fall (approximately 10–20%). The shape of the line plotted for the CA fraction was similar to the shape of the line plotted for the BC + BrC fraction in Beijing (similar in spring and fall; highest in winter). Similarly, Zhai et al. (2021) found that the mass of surface BC continuously decreased from January to May and increased again from October to December in 2016. The Dust fraction was very high (18.9%) in winter (Fig. 9b). The Dust fractions derived from satellite and ground data slightly differed (Figs. 8 and 9), reaching a maximum in spring according to ground data (Fig. 8b), and in winter according to satellite data (Fig. 9b). Zhang and Li (2019) found that desert dust aerosols were most common in spring in Beijing, but Nam et al. (2018) reported that northeast China had the highest PM₁₀ in winter. The coarse size of dust particles can significantly contribute to PM₁₀ (e.g., Querol et al., 2009), which may explain the Dust fraction results in winter.

In Japan, the fraction of LOW reached >80% in fall and winter

(Fig. 9c). The ground data indicated a LOW fraction of >80% in fall and winter (Fig. 8c). The highest percentage of LOW aerosols in Japan occurred in fall, whereas the lowest LOW fraction occurred in spring and summer. Similarly, Nam et al. (2018) discovered that the MODIS AOD was highest in April, May, and June of 2004–2014 in a large area that included Japan. The NA fraction was 34.8% in spring and 36.8% in summer according to satellite data (Fig. 9c), whereas the NA fraction was <15% according to ground data (Fig. 8c). Similar to our NA results, the fine AOD in the Seto Inland Sea region of Japan was higher between March and August than in other months during 2018–2020 (Itahashi et al., 2021). The other aerosol types showed minimal seasonal variation in Japan.

These seasonal results allowed us to identify similar characteristics among ground sites and countries. In all countries, the NA and LOW fractions represented the largest proportion of all aerosols. Similar LOW fractions were observed in ground and satellite data. All ground data showed the highest LOW fraction in fall and winter, whereas satellite data showed that all countries were cleanest in fall. Considering the results of previous studies, this seasonal difference was likely related to differences in coverage between ground and satellite data. Data from Korea showed that the LOW fraction was 30–75%, whereas it was 55–95% for Japan and 20–75% for China, according to both ground and satellite data. The CA fraction had the greatest influence in winter among all countries.

However, we also detected differences between ground and satellite data. Notably, the NA aerosol characteristics slightly differed between ground and satellite data. The seasonal distributions of NA and BC according to satellite data were closer than the seasonal distributions of NA and BC + BrC according to ground data. Seasonal data showed that the sum of the BC and NA fractions in ground data was similar to the size of the NA fraction in satellite data. These results may have been influenced by the criteria used to distinguish between CA and NA aerosols. Because the aerosol types used in this study were classified according to their optical characteristics, some CA may have been misclassified as NA aerosols because of the parameter range used.

The Dust fraction was the dominant aerosol in China in winter according to satellite data, and in spring according to ground data. This seasonal characteristic of the Dust fraction appears to have been caused by regional differences between urban and suburban observation regions. For example, East Asia is mainly affected by yellow dust due to the movement of migratory anticyclones in spring (Takemi and Seino, 2005). Yellow dust is frequently observed even in winter (Chen et al., 2016a, 2016b); it is sometimes also observed in Korea (Kim and Park, 2001). However, in this study, the Dust fraction rarely appeared in Korea in winter (<1%), according to seasonal satellite data. The rapid synoptic flow of yellow dust in winter leads to lower pollution concentrations and shorter duration pollution events, compared with spring (Kim and Park, 2001). Therefore, this phenomenon may not be detected by polar-orbit satellites with short observation times. Differences in the seasonal frequency of the Dust fraction may also have been caused by the use of AOD weighting in the satellite data algorithm. Even if yellow dust passes through the observation range of the satellite, the algorithm may not be able to detect the Dust fraction if it is present over an insufficient AOD_{sum} and area. Thus, suburban regional characteristics may mask the effects of pollution in small areas, overrepresenting the NA fraction in satellite data analyses. The characteristics of this method may explain why the NA aerosol type was particularly overrepresented in the analysis of satellite data.

4. Discussion & Summary

In this study, we analyzed trends in aerosol parameters and aerosol types for three sites (ground data) and three countries (satellite data) in East Asia during 2012–2019. We detected significant decreases in AOD₅₅₀, and AE values in all satellite data. The modified aerosol classification algorithms used in this study revealed annual and seasonal

variations in the dominant aerosol types. Annual aerosol type analysis showed that the fraction of LOW increased at most ground sites. At the Seoul and Osaka sites, the fractions of LOW increased, whereas those of BC + BrC decreased. In Seoul, the fraction of LOW increased from 48.9% to 70.0% during the study period, and that of BC + BrC continuously decreased from 20.4% to 11.1%. Conversely, at the Beijing site, the fraction of LOW decreased from 83.3% (2012) to 52.0% (2019), and that of BC + BrC significantly increased from 2.4% (2013) to 26.2% (2018). Satellite data showed that the fraction of LOW continuously increased in Korea, China, and Japan, whereas that of NA aerosols continuously decreased in all countries. A noticeable decrease in the fraction of BC was also detected in China.

The seasonal aerosol type analysis revealed higher proportions of LOW in fall and winter than in spring and summer at all ground sites. The fractions of BC and NA were present in larger proportions in summer than in the other seasons, according to ground data. For BC + BrC, spring was the most influential season at all ground sites. In all country regions, the CA and NA fractions had the greatest effect in winter and summer, respectively.

The decrease in the BC + BrC fraction in ground data and the decrease in the NA fraction in satellite data contributed most to the increase in the LOW fraction observed in this study. Decreases in AOD, FMF, and AE could indicate decreasing levels of fine particle pollution; such decreases may therefore be related to decreases in pollutant emissions that result from air-quality regulations. A decreasing SSA can be related to an increase/decrease in high/low-absorbing particles, and it may be related to a decrease in pollution. Furthermore, although the BC fraction increased, the decrease in the AAOD of BC may be related to the increasing SSA value in Beijing. In particular, the continuous decrease in NA in all countries was presumably related to the continuous changes in emission characteristics at the global scale that have resulted from improved air-quality regulation, as observed for SO₂. Therefore, changes in aerosol types in East Asia appear to affect the trends in aerosol parameters.

Some of our results were difficult to interpret, such as the differences within a single country. China and Beijing displayed different trends, which could be explained by the gap between urban and suburban characteristics. We also detected significant differences in the NA and BC fractions between ground and satellite data, which may have been related to differences in observation methods (i.e., specific points and wide areas, respectively). Additionally, the Dust fraction was the dominant aerosol in China in winter according to satellite data, and in spring according to ground data. This seasonal characteristic of the Dust fraction was presumably caused by regional differences in urban and suburban observation regions. Further analyses are needed using more ground data from suburban areas to address this discrepancy.

In this study, each aerosol type was observed at all sampling points, and some types showed similar tendencies. Changes in aerosol type may explain the increasing and decreasing trends that we observed for most parameters. In both ground and satellite data, several variations in aerosol types and trends in aerosol parameters occurred concurrently. The data analyses conducted in this study allowed us to draw conclusions based on both datasets. This study demonstrated that consistent results could be obtained using remote-sensing data from ground and satellite observations. We also confirmed that aerosol type classification could be achieved using optical data without direct analysis, based on in situ observations. Therefore, as shown in this study, changes in aerosol types in many areas can easily be identified using optical data via remote sensing. Because remote sensing enables convenient acquisition of observation data for large areas, this technique is expected to be used with increasing regularity in future studies of aerosol types.

CRedit authorship contribution statement

Sujin Eom: Methodology, Formal analysis, Writing – original draft, Writing – review & editing, Visualization, Validation. **Jhoon Kim:** Data

curation, Formal analysis, Resources, Writing – review & editing. **Seoyoung Lee:** Methodology, Data curation, Writing – review & editing, Visualization, Validation. **Brent N. Holben:** Methodology, Software, Validation, Resources, Data curation. **Thomas F. Eck:** Methodology, Software, Validation, Resources, Data curation, Writing – review & editing. **Sung-Bin Park:** Validation, Investigation. **Sang Seo Park:** Conceptualization, Methodology, Validation, Resources, Data curation, Formal analysis, Writing – original draft, Writing – review & editing, Funding acquisition.

Declaration of Competing Interest

The authors declare that they have no known competing financial interests or personal relationships that could have appeared to influence the work reported in this paper.

Data availability

The data that has been used is confidential.

Acknowledgements

This work has supported by the National Research Foundation of Korea (NRF) grant funded by the Korea Government (MSIT) (NRF-2020R1C1C1013628) and supported by the research fund of UNIST (Ulsan National Institute of Science & Technology) (No. 1.190139.01). We acknowledge the NASA Earth Science Division, S-NPP/VIIRS and Aura/OMI science team for the high-quality products. The authors thank all the researchers and staff for establishing and maintaining the AERONET sites used in this study.

References

- Ahmad, S.P., Torres, O., Bhartia, P., Leptoukh, G., Kempler, S., 2006. Aerosol index from TOMS and OMI measurements. In: Proc. of the 86th AMS Annual Meeting.
- Cappa, C.D., Kolesar, K.R., Zhang, X., Atkinson, D.B., Pekour, M.S., Zaveri, R.A., Zelenyuk, A., Zhang, Q., 2016. Understanding the optical properties of ambient sub- and supermicron particulate matter: results from the CARES 2010 field study in northern California. *Atmos. Chem. Phys.* 16, 6511–6535. <https://doi.org/10.5194/acp-16-6511-2016>.
- Cazorla, A., Bahadur, R., Suski, K.J., Cahill, J.F., Chand, D., Schmid, B., Ramanathan, V., Prather, K.A., 2013. Relating aerosol absorption due to soot, organic carbon, and dust to emission sources determined from in-situ chemical measurements. *Atmos. Chem. Phys.* 13, 9337–9350. <https://doi.org/10.5194/acp-13-9337-2013>.
- Chen, Q.X., Yuan, Y., Shuai, Y., Tan, H.P., 2016a. Graphical aerosol classification method using aerosol relative optical depth. *Atmos. Environ.* 135, 84–91. <https://doi.org/10.1016/j.atmosenv.2016.03.061>.
- Chen, Y., Cao, J., Huang, R., Yang, F., Wang, Q., Wang, Y., 2016b. Characterization, mixing state, and evolution of urban single particles in Xi'an (China) during wintertime haze days. *Sci. Total Environ.* 573 (2016), 937–945. <https://doi.org/10.1016/j.scitotenv.2016.08.151>.
- Chen, Q.X., Huang, C.L., Yuan, Y., Mao, Q.J., Tan, H.P., 2020. Spatiotemporal distribution of Major Aerosol Types over China based on MODIS Products between 2008 and 2017. *Atmosphere* 11 (7), 703. <https://doi.org/10.3390/atmos11070703>.
- China State Council, 2013. Action Plan on Prevention and Control of Air Pollution. China State Council, Beijing, China. http://www.gov.cn/zwqk/2013-09/12/content_2486773.
- Cho, J.H., Kim, H.S., Chung, Y.S., 2021. Spatio-temporal changes of PM10 trends in South Korea caused by East Asian atmospheric variability. *Air Qual. Atmos. Health* 14, 1001–1016. <https://doi.org/10.1007/s11869-021-00995-y>.
- Choi, Y., Ghim, Y.S., Holben, B.N., 2016. Identification of columnar aerosol types under high aerosol optical depth conditions for a single AERONET site in Korea. *J. Geophys. Res.* Atmos. 121, 1264–1277. <https://doi.org/10.1002/2015JD024115>.
- Choi, Y., Ghim, Y.S., Zhang, Y., Park, S.M., Song, I.H., 2020. Estimation of Surface Concentrations of Black Carbon from Long-Term Measurements at Aeronet Sites over Korea. *Remote Sens.* 12 (23), 3904. <https://doi.org/10.3390/rs12233904>.
- de Vries, M.J.M.P., Beirle, S., Hormann, C., Kaiser, J.W., Stammes, P., Tilstra, L.G., Tuinder, O.N.E., Wagner, T., 2015. A global aerosol classification algorithm incorporating multiple satellite data sets of aerosol and trace gas abundances. *Atmos. Chem. Phys.* 15, 10597–10618. <https://doi.org/10.5194/acp-15-10597-2015>.
- Dehkoda, N., Noh, Y., Joo, S., 2020. Long-Term Variation of Black Carbon Absorption Aerosol Optical Depth from AERONET Data over East Asia. *Remote Sens.* 12 (21), 3551. <https://doi.org/10.3390/rs12213551>.
- Diapoulis, E., Popovicheva, O., Kistler, M., Vratolis, S., Persiantseva, N., Timofeev, M., Kasper-Giebl, A., Eleftheriadis, K., 2014. Physicochemical characterization of aged biomass burning aerosol after long-range transport to Greece from large scale wildfires in Russia and surrounding regions, summer 2010. *Atmos. Environ.* 96, 393–940. <https://doi.org/10.1016/j.atmosenv.2014.07>.
- Dingenen, R.V., Raes, F., Putaud, J.P., Baltensperger, U., Charron, A., Facchini, M.C., Decesari, S., Fuzzi, S., Gehrig, R., Hansson, H.C., Harrison, R.M., Hüglin, C., Jones, A.M., Laj, P., Lorbeer, G., Maenhaut, W., Palmgren, F., Querol, X., Rodriguez, S., Schneider, J., Brink, H.T., Tunved, P., Torseth, K., Wehner, B., Weigartner, E., Wiedensohler, A., Wahlin, P., 2004. A European aerosol phenomenology—1: physical characteristics of particulate matter at kerbside, urban, rural and background sites in Europe. *Atmos. Environ.* 38 (2004), 2561–2577. <https://doi.org/10.1016/j.atmosenv.2004.01.040>.
- Dubovik, O., King, M.D., 2000. A flexible inversion algorithm for retrieval of aerosol optical properties from Sun and sky radiance measurements. *J. Geophys. Res.* 105 (D16), 20673–20696. <https://doi.org/10.1029/2000JD900282>.
- Dubovik, O., Smirnov, A., Holben, B.N., King, M.D., Kaufman, Y.J., Eck, T.F., Slutsker, I., 2000. Accuracy assessments of aerosol optical properties retrieved from Aerosol Robotic Network (AERONET) Sun and sky radiance measurements. *J. Geophys. Res.* 105 (D8), 9791–9806. <https://doi.org/10.1029/2000JD900040>.
- Dubovik, O., Sinyuk, A., Lapyonok, T., Holben, B.N., Mishchenko, M., Yang, P., Eck, T.F., Volten, H., Muñoz, O., Veihelmann, B., van der Zande, W.J., Leon, J., Sorokin, M., Slutsker, I., 2006. Application of spheroid models to account for aerosol particle nonsphericity in remote sensing of desert dust. *J. Geophys. Res.* 111 (D11) <https://doi.org/10.1029/2005JD006619>.
- Dudley, B., 2018. 2018. BP Statistical Review of World Energy. BP Statistical Review, London, UK. accessed Aug, 6, p. 00116.
- Eck, T.F., Holben, B.N., Reid, J.S., Dubovik, O., Smirnov, A., O'Neill, N.T., Slutsker, I., Kinne, S., 1999. Wavelength dependence of the optical depth of biomass burning, urban, and desert dust aerosols. *J. Geophys. Res.* 104 (D24), 31333–31349. <https://doi.org/10.1029/1999JD900923>.
- Eck, T.F., Holben, B.N., Dubovik, O., Smirnov, A., Goloub, P., Chen, H.B., Chatenet, B., Gomes, L., Zhang, X.-Y., Tsay, S.-C., Ji, Q., Giles, D., Slutsker, I., 2005. Columnar aerosol optical properties at AERONET sites in central-eastern Asia and aerosol transport to the tropical mid-Pacific. *J. Geophys. Res.* 110, D06202. <https://doi.org/10.1029/2004JD005274>.
- Eck, T.F., Holben, B.N., Reid, J.S., Mukelabai, M.M., Piketh, S.J., Torres, O., Jethva, H.T., Hyer, E.J., Ward, D.E., Dubovik, O., Sinyuk, A., Schafer, J.S., Giles, D.M., Sorokin, M., Smirnov, A., Slutsker, I., 2013. A seasonal trend of single scattering albedo in southern African biomass-burning particles: Implications for satellite products and estimates of emissions for the world's largest biomass-burning source. *J. Geophys. Res.: Atmospheres*. 118, 6414–6432. <https://doi.org/10.1002/jgrd.50500>.
- Eck, T.F., Holben, B.N., Giles, D.M., Slutsker, I., Sinyuk, A., Schafer, J.S., Smirnov, A., Sorokin, M., Reid, J.S., Sayer, A.M., Hsu, N.C., Shi, Y.R., Levy, R.C., Lyapustin, A., Rahman, M.A., Liew, S.C., Cortijo, S.V.S., Li, T., Kalbermatter, D., Keong, K.L., Yunggotomo, M.E., Aditya, F., Mohamad, M., Mahmud, M., Chong, T.K., Lim, H.S., Choon, Y.E., Deranadayan, G., Kusumaningtyas, S.D.A., Aldrian, E., 2019. AERONET Remotely Sensed Measurements and Retrievals of Biomass burning Aerosol Optical Properties during the 2015 Indonesian burning season. *J. Geophys. Res.: Atmospheres*. 124, 4722–4740. <https://doi.org/10.1029/2018JD030182>.
- Gen, M., Zhang, R., Huang, D.D., Li, Y., Chan, C.K., 2019. Heterogeneous SO₂ Oxidation in Sulfate Formation by Photolysis of Particulate Nitrate. *Environ. Sci. Technol. Lett.* 6 (2019), 86–91. <https://doi.org/10.1021/acs.estlett.8b00681>.
- Giles, D.M., Holben, B.N., Eck, T.F., Sinyuk, A., Smirnov, A., Slutsker, I., Dickerson, R.R., Thompson, A.M., Schafer, J.S., 2012. An analysis of AERONET aerosol absorption properties and classifications representative of aerosol source regions. *J. Geophys. Res.* 117 (D17203) <https://doi.org/10.1029/2012JD018127>.
- Giles, D.M., Sinyuk, A., Sorokin, M.G., Schafer, J.S., Smirnov, A., Slutsker, I., Eck, T.F., Holben, B.N., Lewis, J.R., Campbell, J.R., Welton, E.J., Korkin, S.V., Lyapustin, A.I., 2019. Advancements in the Aerosol Robotic Network (AERONET) Version 3 database—Automated near-real-time quality control algorithm with improved cloud screening for Sun photometer aerosol optical depth (AOD) measurements. *Atmos. Meas. Tech.* 12, 169–209. <https://doi.org/10.5194/amt-12-169-2019>.
- Givati, A., Rosenfeld, D., 2007. Possible impacts of anthropogenic aerosols on water resources of the Jordan River and the Sea of Galilee. *Water Resour. Res.* 43, W10419. <https://doi.org/10.1029/2006WR005771>.
- Guo, J.P., Zhang, X.Y., Wu, Y.R., Zhaxi, W., Che, H., La, Z., Wang, B., Li, W., 2011. Spatio-temporal variation trends of satellite-based aerosol optical depth in China during 1980–2008. *Atmos. Environ.* 45 (2011), 6802–6811.
- Hamill, P., Giordano, M., Ward, C., Giles, D., Holben, B., 2016. An AERONET-based aerosol classification using the Mahalanobis distance. *Atmos. Environ.* 140 (2016), 213–233. <https://doi.org/10.1016/j.atmosenv.2016.06.002>.
- Higurashi, A., Nakajima, T., 2002. Detection of aerosol types over the East China Sea near Japan from four-channel satellite data. *Geophys. Res. Lett.* 29 (17), 1836. <https://doi.org/10.1029/2002GL015357>.
- Ho, C.H., Heo, J.W., Chang, M., Choi, W., Kim, J., Kim, S.W., Oh, H.R., 2021. Regulatory measures significantly reduced air-pollutant concentrations in Seoul. *Korea. Atmos. Pollut. Res.* 12 (7), 101098. <https://doi.org/10.1016/j.apr.2021.101098>.
- Holben, B.N., Eck, T.F., Slutsker, I., Tanre, D., Buis, J.P., Setzer, A., Vermote, E., Reagan, J.A., Kaufman, Y.J., Nakajima, T., Lavenue, F., Jankowiak, I., Smirnov, A., 1998. AERONET—A Federated Instrument Network and Data Archive for Aerosol Characterization. *Remote Sens. Environ.* 66 (1), 1–16.
- Hopner, F., Bender, F.A.M., Ekman, A.M.L., Andersson, A., Gustafsson, O., Leck, C., 2018. Investigation of two Optical Methods for Aerosol-Type Classification Extended to a Northern Indian Ocean Site. *J. Geophys. Res.: Atmospheres*. 124, 8743–8763. <https://doi.org/10.1029/2018JD029685>.

- Hsu, N.C., Lee, J., Sayer, A.M., Kim, W., Bettenhausen, C., Tsay, S.-C., 2019. VIIRS Deep Blue Aerosol Products over Land: Extending the EOS Long-Term Aerosol Data Records. *J. Geophys. Res.: Atmospheres*. 124, 4026–4053. <https://doi.org/10.1029/2018JD029688>.
- Itahashi, S., Sakurai, T., Shimadera, H., Araki, S., Hayami, H., 2021. Long-term trends of satellite-based fine-mode aerosol optical depth over the Seto Inland Sea, Japan, over two decades (2001–2020). *Environ. Res. Lett.* 16 (2021), 064062 <https://doi.org/10.1088/1748-9326/ac03db>.
- Kang, L., Chen, S., Huang, J., Zhao, S., Ma, X., Yuan, T., Zhang, X., Xie, T., 2017. The spatial and temporal distributions of absorbing aerosols over East Asia. *Remote Sens.* 9 (10), 1050. <https://doi.org/10.3390/rs9101050>.
- Kaskaoutis, D.G., Badarinarayana, K.V.S., Kharol, S.K., Sharma, A.R., Kambezidis, H., 2009. Variations in the aerosol optical properties and types over the tropical urban site of Hyderabad, India. *J. Geophys. Res.* 114 (D22204) <https://doi.org/10.1029/2009JD012423>.
- Kaskaoutis, D.G., Grivas, G., Stavroulas, I., Liakakou, E., Dumka, U.C., Dimitriou, K., Gerasopoulos, E., Mihalopoulos, N., 2021. In situ identification of aerosol types in Athens, Greece, based on long-term optical and on online chemical characterization. *Atmos. Environ.* 246, 118070 <https://doi.org/10.1016/j.atmosenv.2020.118070>.
- Kedia, S., Ramachandran, S., Holben, B.N., Tripathi, S.N., 2014. Quantification of aerosol type, and sources of aerosols over the Indo-Gangetic Plain. *Atmos. Environ.* 98, 607–619. <https://doi.org/10.1016/j.atmosenv.2014.09.022>.
- Kim, B.G., Park, S.U., 2001. Transport and evolution of a winter-time Yellow sand observed in Korea. *Atmos. Environ.* 35 (2001), 3191–3201. [https://doi.org/10.1016/S1352-2310\(00\)00469-6](https://doi.org/10.1016/S1352-2310(00)00469-6).
- Kim, J., Lee, J., Lee, H.C., Higurashi, A., Takemura, T., Song, C.H., 2007. Consistency of the aerosol type classification from satellite remote sensing during the Atmospheric Brown Cloud–East Asia Regional Experiment campaign. *J. Geophys. Res.* 112 (D22533) <https://doi.org/10.1029/2006JD008201>.
- Kim, H.S., Chung, Y.S., Kim, J.T., 2014. Spatio-Temporal Variations of Optical Properties of Aerosols in East Asia measured by MODIS and Relation to the Ground-based Mass Concentrations Observed in Central Korea during 2001–2010. *Asia-Pac. J. Atmos. Sci.* 50 (2), 191–200. <https://doi.org/10.1007/s13143-014-0007-8>.
- Koch, D., Menon, S., Geino, A.D., Ruedy, R., Alienov, I., Schmidt, G.A., 2009. Distinguishing Aerosol Impacts on climate over the Past Century. *J. Clim.* 22 (10), 2659–2677. <https://doi.org/10.1175/2008JCLI2573.1>.
- Kurokawa, J., Ohara, T., 2020. Long-term historical trends in air pollutant emissions in Asia: Regional Emission inventory in Asia (REAS) version 3. *Atmos. Chem. Phys.* 20, 12761–12793. <https://doi.org/10.5194/acp-20-12761-2020>.
- Kwon, H.J., Cho, S.H., Chun, Y.S., Lagarde, F., Pershagen, G., 2002. Effects of the Asian Dust events on Daily Mortality in Seoul, Korea. *Environ. Res.* 90, 1–5. <https://doi.org/10.1006/enrs.2002.4377>.
- Lee, K.H., Kim, Y.J., 2010. Satellite remote sensing of Asian aerosols: a case study of clean, polluted, and Asian dust storm days. *Atmos. Meas. Tech.* 3, 1771–1784. <https://doi.org/10.5194/amt-3-1771-2010>.
- Lee, J., Kim, J., Lee, H.C., Takemura, T., 2007. Classification of Aerosol Type from MODIS and OMI over East Asia. *Asia-Pac. J. Atmos. Sci.* 43 (4), 343–357.
- Lee, J., Kim, J., Song, C.H., Kim, S.B., Chun, Y., Sohn, B.J., Holben, B.N., 2010. Characteristics of aerosol types from AERONET sunphotometer measurements. *Atmos. Environ.* 44 (2010), 3110–3117. <https://doi.org/10.1016/j.atmosenv.2010.05.035>.
- Lee, S., Hong, J., Cho, Y., Choi, M., Kim, J., Park, S.S., Ahn, J.Y., Kim, S.K., Moon, K.J., Eck, T.F., Holben, B.N., Koo, J.H., 2018a. Characteristics of Classified Aerosol Types in South Korea during the MAPS-Seoul Campaign. *Aerosol Air Qual. Res.* 18, 2195–2206. <https://doi.org/10.4209/aaqr.2017.11.0474>.
- Lee, S., Yoo, H., Nam, M., 2018b. Impact of the Clean Air Act on air pollution and infant health: evidence from South Korea. *Econ. Lett.* 168, 98–101. <https://doi.org/10.1016/j.econlet.2018.04.010>.
- Lee, J., Koo, J.H., Kim, S.M., Lee, T., Lee, Y.G., 2021. Asia-Pacific. *J. Atmos. Sci.* 57, 629–643. <https://doi.org/10.1007/s13143-020-00221-2>.
- Lei, Y., Zhang, Q., He, K.B., Streets, D.G., 2011. Primary anthropogenic aerosol emission trends for China, 1990–2005. *Atmos. Chem. Phys.* 11, 931–954. <https://doi.org/10.5194/acp-11-931-2011>.
- Li, J., 2020. Pollution Trends in China from 2000 to 2017: a Multi-Sensor View from Space. *Remote Sens.* 12 (2), 208. <https://doi.org/10.3390/rs12020208>.
- Li, J., Carlson, B.E., Dubovik, O., Laci, A.A., 2014. Recent trends in aerosol optical properties derived from AERONET measurements. *Atmos. Chem. Phys.* 14, 12271–12289. <https://doi.org/10.5194/acp-14-12271-2014>.
- Li, W., Shao, L., Zhang, D., Ro, C.U., Hu, M., Bi, X., Geng, H., Matsuki, A., Niu, H., Chen, J., 2015. A review of single aerosol particle studies in the atmosphere of East Asia: morphology, mixing state, source, and heterogeneous reactions. *J. Clean. Prod.* 112 (2016), 1330–1349. <https://doi.org/10.1016/j.jclepro.2015.04.050>.
- Li, L., Che, H., Zhang, X., Chen, C., Chen, X., Gui, K., Liang, Y., Wang, F., Derimian, Y., Fuentes, D., Dubovik, O., Zheng, Y., Zhang, L., Guo, B., Wang, Y., Zhang, X., 2022. A satellite-measured view of aerosol component content and optical property in a haze-polluted case over North China Plain. *Atmos. Res.* 266 (2022), 105958 <https://doi.org/10.1016/j.atmosres.2021.105958>.
- Lin, Y., Tian, P., Tang, C., Pang, S., Zhang, L., 2022. Combining CALIPSO and AERONET Data to Classify Aerosols Globally. *IEEE Trans. Geosci. Remote Sens.* 60, 1–12. <https://doi.org/10.1109/TGRS.2021.3138085>.
- Liu, Y., Lin, T., Hong, J., Wang, Y., Shi, L., Huang, Y., Wu, X., Zhou, H., Zhang, J., de Leeuw, G., 2021. Multi-dimensional satellite observations of aerosol properties and aerosol types over three major urban clusters in eastern China. *Atmos. Chem. Phys.* 21, 12331–12358. <https://doi.org/10.5194/acp-21-12331-2021>.
- Logothetis, et al., 2020. Aerosol classification in Europe, Middle East, North Africa and Arabian Peninsula based on AERONET Version 3.
- Malilay, J., 1999. A Review of Factors Affecting the Human Health Impacts of Air Pollutants from Forest Fires. *Health Guidelines for Vegetation Fire Events: Background Papers*, pp. 255–270.
- Mok, J.B., Park, S.S., Lim, H.K., Kim, J., Edwards, D.P., Lee, J., Yoon, J., Lee, Y.G., Koo, J. H., 2017. Correlation analysis between regional carbon monoxide and black carbon from satellite measurements. *Atmos. Res.* 196 (2017), 29–39. <https://doi.org/10.1016/j.atmosres.2017.04.004>.
- Nagorski, S., Kaspari, S., Hood, E., Fellman, J.B., Skiles, S.M., 2018. Radiative Forcing by Dust and Black Carbon on the Juneau Icefield, Alaska. *J. Geophys. Res.* : Atmospheres. 124, 3943–3959. <https://doi.org/10.1029/2018JD02941>.
- Nam, J., Kim, S.W., Park, R.J., Park, J.S., Park, S.S., 2018. Changes in column aerosol optical depth and ground-level particulate matter concentration over East Asia. *Air Qual. Atmos. Health* 11, 49–60. <https://doi.org/10.1007/s11869-017-0517-5>.
- Nguyen, T.T.N., Pham, H.V., Lasko, K., Bui, M.T., Laffly, D., Jourdan, A., Bui, H.Q., 2019. Spatiotemporal analysis of ground and satellite-based aerosol for air quality assessment in the Southeast Asia region. *Environ. Pollution*. 255 (2019), 113106 <https://doi.org/10.1016/j.envpol.2019.113106>.
- Omar, A.H., Won, J.G., Winker, D.M., Yoon, S.C., Dubovik, O., McCormick, M.P., 2005. Development of global aerosol models using cluster analysis of Aerosol Robotic Network (AERONET) measurements. *J. Geophys. Res.* 110 (D10S14) <https://doi.org/10.1029/2004JD004874>.
- Ou, Y., Zhao, W., Wang, J., Zhao, W., Zhang, B., 2017. Characteristics of Aerosol Types in Beijing and the Associations with Air Pollution from 2004 to 2015. *Remote Sens.* 9 (9), 898. <https://doi.org/10.3390/rs9090898>.
- Park, R.J., Jacob, D.J., Chin, M., Martin, R.V., 2003. Sources of carbonaceous aerosols over the United States and implications for natural visibility. *J. Geophys. Res.* 108 (D12), 4355. <https://doi.org/10.1029/2002JD003190>.
- Provencal, S., Kishcha, P., da Silva, A.M., Elhacham, E., Alpert, P., 2017. AOD distributions and trends of major aerosol species over a selection of the world's most populated cities based on the 1st version of NASA's MERRA Aerosol Reanalysis. *Urban Climate*. 20 (2017), 168–191. <https://doi.org/10.1016/j.uclim.2017.04.001>.
- Querol, X., Pey, J., Pandolfi, M., Alastuey, A., Cusack, M., Perez, N., Moreno, T., Viana, M., Mihalopoulos, N., Kallos, G., Kleanthous, S., 2009. *Atmos. Environ.* 43 (28), 4266–4277. <https://doi.org/10.1016/j.atmosenv.2009.06.013>.
- Quinn, P.K., Coffman, D.J., Bates, T.S., Welton, E.J., Covert, D.S., Miller, T.L., Johnson, J. E., Maria, S., Russell, L., Arimoto, R., Carrico, C.M., Rood, M.J., Anderson, J., 2004. Aerosol optical properties measured on board the Ronald H. Brown during ACE-Asia as a function of aerosol chemical composition and source region. *J. Geophys. Res.* 109 (D19S01) <https://doi.org/10.1029/2003JD004010>.
- Ramachandran, S., Rupakheti, M., Lawrence, M.G., 2020. Aerosol-induced atmospheric heating rate decreases over South and East Asia as a result of changing content and composition. *Scientific Rep.* 10 (1), 1–17.
- Rap, A., Scott, C.E., Spracklen, D.V., Bellouin, N., Forster, P.M., Carslaw, K.S., Schmidt, A., Mann, G., 2013. Natural aerosol direct and indirect radiative effects. *Geophys. Res. Lett.* 40, 3297–3301. <https://doi.org/10.1002/grl.50441>.
- Reid, J.S., Koppmann, R., Eck, T., Eleuterio, D., 2005. A review of biomass burning emissions: Part II. Intensive physical properties of biomass burning particles. *Atmos. Chem. Phys.* 5, 799–825. <https://doi.org/10.5194/acp-5-799-2005>.
- Ronald, Van Der A., Mijling, B., Ding, J., Koukoulis, M.E., Liu, F., Li, Q., Mao, H., Theys, N., 2017. Cleaning up the air: effectiveness of air quality policy for SO₂ and NO_x emissions in China. *Atmos. Chem. Phys.* 17, 1775–1789. <https://doi.org/10.5194/acp-17-1775-2017>.
- Schmeisser, L., Andrews, E., Ogren, J.A., Sheridan, P., Jefferson, A., Sharma, S., Kim, J. E., Sherman, J.P., Sorribas, M., Kalapov, I., Arsov, T., Angelov, C., Mayol-Bracero, O. L., Labuschagne, C., Kim, S.W., Hoffer, A., Lin, N.H., Chia, H.P., Bergin, M., Sun, J., Liu, P., Wu, H., 2017. Classifying aerosol type using in situ surface spectral aerosol optical properties. *Atmos. Chem. Phys.* 17, 12097–12120. <https://doi.org/10.5194/acp-17-12097-2017>.
- Schreifels, J.J., Fu, Y., Wilson, E.J., 2012. Sulfur dioxide control in China: policy evolution during the 10th and 11th Five-year Plans and lessons for the future. *Energy Policy* 48, 779–789. <https://doi.org/10.1016/j.enpol.2012.06.015>.
- Segerström, D., Eneroth, K., Gidhagen, L., Johansson, C., Omstedt, G., Nylen, A.E., Forsberg, B., 2017. Health Impact of PM₁₀, PM_{2.5} and Black Carbon Exposure due to different Source Sectors in Stockholm, Gothenburg and Umea, Sweden. *Int. J. Environ. Res. Public Health* 14 (7), 742. <https://doi.org/10.3390/ijerph14070742>.
- Seoul Air Quality Report, 2021. Seoul Institute Health, Seoul, Korea. <https://cleanair.seoul.go.kr>.
- Shao, Y., Dong, C.H., 2006. A review on East Asian dust storm climate, modelling and monitoring. *Glob. Planet. Chang.* 52 (1–4), 1–22. <https://doi.org/10.1016/j.gloplacha.2006.02.011>.
- Shin, S.K., Tesche, M., Noh, Y., Müller, D., 2019. Aerosol-type classification based on AERONET version 3 inversion products. *Atmos. Meas. Tech.* 12, 3789–3803. <https://doi.org/10.5194/amt-12-3789-2019>.
- Singh, A., Rastogi, N., 2019. Quantification of organic carbon from biomass versus non-biomass burning emissions to fine aerosol. *Proc. Indian Nat. Sci. Acad.* 85, 629–636. <https://doi.org/10.16943/ptinsa/2019/49585>.
- Sinyuk, A., Holben, B.N., Eck, T.F., Giles, D.M., Slutsker, I., Korkin, S., Schafer, J.S., Smirnov, A., Sorokin, M., Lyapustin, A., 2020. The AERONET Version 3 aerosol retrieval algorithm associated uncertainties and comparison to Version 2. *Atmos. Meas. Tech.* 13, 3375–3411. <https://doi.org/10.5194/amt-13-3375-2020>.
- Smith, S.J., Pitcher, H., Wigley, T.M.L., 2001. Global and regional anthropogenic sulfur dioxide emissions. *Glob. Planet. Change* 29 (2001), 99–119. [https://doi.org/10.1016/S0921-8181\(00\)00057-6](https://doi.org/10.1016/S0921-8181(00)00057-6).
- Song, C.H., Park, M.E., Lee, K.H., Ahn, H.J., Lee, Y., Kim, J.Y., Han, K.M., Kim, J., Ghim, Y.S., Kim, Y.J., 2008. An investigation into seasonal and regional aerosol characteristics in East Asia using model-predicted and remotely-sensed aerosol

- properties. *Atmos. Chem. Phys.* 8, 6627–6654. <https://doi.org/10.5194/acp-8-6627-2008>.
- Song, Z., Fu, D., Zhang, X., Wu, Y., Xia, X., He, J., Han, X., Zhang, R., Che, H., 2018. Diurnal and seasonal variability of PM_{2.5} and AOD in North China plain: Comparison of MERRA-2 products and ground measurements. *Atmos. Environ.* 191 (2018), 70–78. <https://doi.org/10.1016/j.atmosenv.2018.08.012>.
- Streets, D.G., Yan, F., Chin, M., Diehl, T., Mahowald, N., Schultz, M., Wild, M., Wu, Y., Yu, C., 2009. Anthropogenic and natural contributions to regional trends in aerosol optical depth, 1980–2006. *J. Geophys. Res.* 114 (D10) <https://doi.org/10.1029/2008JD011624>.
- Sun, J., Wang, Z., Zhou, W., Xie, C., Wu, C., Chen, C., Han, T., Wang, Q., Li, Z., Li, J., Fu, P., Wang, Z., Sun, Y., 2022. Measurement report: long-term changes in black carbon and aerosol optical properties from 2012 to 2020 in Beijing, China. *Atmos. Chem. Phys.* 22, 561–575. <https://doi.org/10.5194/acp-22-561-2022>.
- Szidat, S., Prevot, A.S.H., Sandradewi, J., Alfarra, M.R., Sýnal, H.-A., Wacker, L., 2007. Dominant impact of residential wood burning on particulate matter in Alpine valleys during winter. *Geophys. Res. Lett.* 34, L05820. <https://doi.org/10.1029/2006GL02832>.
- Takemi, T., Seino, N., 2005. Dust storms and cyclone tracks over the arid regions in East Asia in spring. *JGR. Atmospheres* 110 (D18). <https://doi.org/10.1029/2004JD004698>.
- Tian, Y., Pan, X., Wang, Z., Wang, D., Ge, B., Liu, X., Zhang, Y., Liu, H., Lei, S., Yang, T., Fu, P., Sun, Y., Wang, Z., 2020. Transport patterns, size Distributions, and Depolarization Characteristics of Dust Particles in East Asia in spring 2018. *J. Geophys. Res.: Atmospheres* 125. <https://doi.org/10.1029/2019JD031752>.
- Tie, X., Cao, J., 2009. Aerosol pollution in China: present and future impact on environment. *Particulology*. 7 (2009), 426–431. <https://doi.org/10.1016/j.partic.2009.09.003>.
- Torres, O., Ahn, C., Chen, Z., 2013. Improvements to the OMI near-UV aerosol algorithm using A-train CALIOP and AIRS observations. *Atmos. Meas. Tech.* 6, 3257–3270. <https://doi.org/10.5194/amt-6-3257-2013>.
- Wang, Z., Zhang, M., Wang, L., Feng, L., Ma, Y., Gong, W., Qin, W., 2021. Long-term evolution of clear sky surface solar radiation and its driving factors over East Asia. *Atmos. Environ.* 262 (2021), 118661 <https://doi.org/10.1016/j.atmosenv.2021.118661>.
- Xia, X., 2014. A critical assessment of direct radiative effects of different aerosol types on surface global radiation and its components. *J. Quant. Spectrosc. Radiat. Transf.* 149 (2014), 72–80. <https://doi.org/10.1016/j.jqsrt.2014.07.020>.
- Xia, Q., Zhang, H., Choi, M., Li, S., Kondragunta, S., Kim, J., Holben, B., Levy, R.C., Liu, Y., 2016. Evaluation of VIIRS, GOCI, and MODIS Collection 6 AOD retrievals against ground sunphotometer observations over East Asia. *Atmos. Chem. Phys.* 16, 1255–1269. <https://doi.org/10.5194/acp-16-1255-2016>.
- Yan, X., Zang, Z., Li, Z., Luo, N., Zuo, C., Jiang, Y., Li, D., Guo, Y., Zhao, W., Shi, W., Cribb, M., 2022. A global land aerosol fine-mode fraction dataset (2001–2020) retrieved from MODIS using hybrid physical and deep learning approaches. *Earth Syst. Sci. Data*. 14, 1193–1213. <https://doi.org/10.5194/essd-14-1193-2022>.
- Yin, S., 2021. Decadal trends of MERRA-estimated PM_{2.5} concentrations in East Asia and potential exposure. from 1990 to 2019 *Atmos. Environ.* 264 (2021), 118690. <https://doi.org/10.1016/j.atmosenv.2021.118690>.
- Zhai, S., Jacob, D.J., Wang, X., Shen, L., Li, K., Zhang, Y., Gui, K., Zhao, T., Liao, H., 2019. Fine particulate matter (PM_{2.5}) trends in China, 2013–2018: separating contributions from anthropogenic emissions and meteorology. *Atmos. Chem. Phys.* 19, 11031–11041. <https://doi.org/10.5194/acp-19-11031-2019>.
- Yu, X., Lü, R., Liu, C., Yuan, L., Shao, Y., Zhu, B., Lei, L., 2017. Seasonal variation of columnar aerosol optical properties and radiative forcing over Beijing, China. *Atmos. Environ.* 166, 340–350.
- Zhai, S., Jacob, D.J., Brewer, J.F., Li, K., Moch, J.M., Kim, J., Lee, S., Lim, H., Lee, H.C., Kuk, S.K., Park, R.J., Jeong, J.I., Wang, X., Liu, P., Luo, G., Yu, F., Meng, J., Martin, R.V., Travis, K.R., Hair, J.W., Anderson, B.E., Dibb, J.E., Jimenez, J.L., Campuzano-Jost, P., Nault, B.A., Woo, J.-H., Kim, Y., Zhang, Q., Liao, H., 2021. Relating geostationary satellite measurements of aerosol optical depth (AOD) over East Asia to fine particulate matter (PM_{2.5}): insights from the KORUS-AQ aircraft campaign and GEOS-Chem model simulations. *Atmos. Chem. Phys.* 21, 16775–16791. <https://doi.org/10.5194/acp-21-16775-2021>.
- Zhang, L., Li, J., 2019. Variability of Major Aerosol Types in China Classified using AERONET Measurements. *Remote Sens.* 11 (20), 2334. <https://doi.org/10.3390/rs11202334>.
- Zhao, B., Jiang, J.H., Gu, Y., Diner, D., Worden, J., Liou, K.N., Su, H., Xing, J., Garay, M., Huang, L., 2017. Decadal-scale trends in regional aerosol particle properties and their linkage to emission changes. *Environ. Res. Lett.* 12 (5), 054021 <https://doi.org/10.1088/1748-9326/aa6cb2>.
- Zheng, B., Tong, D., Li, M., Liu, F., Hong, C., Geng, G., Li, H., Li, X., Peng, L., Qi, J., Yan, L., Zhang, Y., Zhao, H., Zheng, Y., He, K., Zhang, Q., 2018. Trends in China's anthropogenic emissions since 2010 as the consequence of clean air actions. *Atmos. Chem. Phys.* 18, 14095–14111. <https://doi.org/10.5194/acp-18-14095-2018>.
- Zhong, Q., Shen, H., Yun, X., Chen, Y., Ren, Y., Xu, H., Shen, G., Du, W., Meng, J., Li, W., Ma, J., Tao, S., 2020. Global Sulfur Dioxide Emissions and the Driving forces. *Environ. Sci. Technol.* 54 (2020), 6508–6517. <https://doi.org/10.1021/acs.est.9b07696>.